REPUBLIQUE ALGERIENNE DEMOCRATIQUE ET POPULAIRE

الجمهورية الجزائرية الديمقراطية الشعبية

MINISTERE DE L'ENSEIGNEMENT SUPERIEUR ET DE LA RECHERCHE SCIENTIFIQUE

ECOLE SUPERIEURE EN SCIENCES APPLIQUEES
--T L E M C E N--

وزارة التعليم العالي والبحث العلمي

المدرسة العليا في العلوم التطبيقية

Mémoire de fin d'étude

Pour l'obtention du diplôme d'Ingénieur

Filière : Électrotechnique

Spécialité : Énergie et environnement

Présenté par : MERIEM Hichem

Thème

Design and Implementation of a Solar-Powered Automatic Mobile Traction Irrigation System SPAMIS

Soutenu publiquement, le 30 septembre 2026, devant le jury composé de :

Mme. Djamila KHERBOUCHE	M.C.A	ESSA Tlemcen	Président de jury
M. Farid OUDJAMA	M.C.B	ESSA Tlemcen	Encadrant
M. Mohammed MESSIRDI	M.C.B	Univ. Mascara	Co-encadrant
Mme. Imen BOUSMAHA	M.C.A	ESSA Tlemcen	Examinateur 1
M. Boulanouar MESSAOUDI	M.C.A	ESSA Tlemcen	CATI

Année universitaire : 2025/2026

Acknowledgement

First and foremost, we thank Allah the Almighty for granting us the health, strength, patience, and perseverance needed to successfully complete this work.

I wish to express my deep gratitude to my supervisor, Dr Farid OUJDAMA, for his constant guidance, availability, and invaluable advice.

I also extend my sincere thanks to my co-supervisor, Dr. Mohammed MESSIRDI, for his insightful guidance and the numerous constructive comments and assistance that contributed to making this work.

A special thanks to Mms MIMOUNI and Mms KHERBOUCHE and for their invaluable contributions and assistance.

My thanks extend to all the faculty, administrative staff, and technical staff at the Higher School of Applied Sciences in Tlemcen, who contributed to my academic training and personal development throughout my university studies. Finally, I extend my gratitude to my family, friends, and colleagues, as well as to everyone who supported, encouraged, and assisted me directly or indirectly in bringing this work to completion.

To one and all, I express my sincere appreciation and deep respect.

Dedication

I dedicate this modest work to my dearly loved parents, who have always been my greatest source of strength, motivation, and inspiration. Thank you for your unconditional love, unwavering support, sacrifices, and all the effort you have made to enable me to reach this stage of my journey. You have always believed in me, even during the most difficult times, and no words can fully express my gratitude and deep respect. May this work serve as a testament to my appreciation and a modest reward for everything you have done for me.

To myself, for the effort put in, the sacrifices made, the challenges overcome, and the perseverance I demonstrated throughout this journey to achieve this goal.

To my entire family, with a special thought of gratitude for my dear uncle Kamel.

To all my friends, and fellow students, for their help, friendship, and the precious moments shared during these years of study.

Finally, I dedicate this work to everyone who contributed, directly or indirectly, to my success and who supported and encouraged me throughout my journey.

To all of you, I express my sincere gratitude and deep respect.

Hichem

Abstract

Lateral move irrigation systems offer efficient, uniform field coverage but typically depend on diesel generators or trailing cables for tower movement which is impractical in off-grid contexts like Saharan Algeria. This thesis designs and validates a photovoltaic and battery powered drive system for lateral move locomotion, excluding the pumping function. The methodology proceeds in four stages: a literature review identifying the lack of battery buffered PV drive solutions; a modular sizing approach applied to a real case study in Tebessa to determine drivetrain and power requirements; validation through three complementary tools PVsyst, LOGO!Soft Comfort, and MATLAB/Simulink; and finally a small scale Arduino based prototype demonstrating autonomous, solar-powered locomotion. Results across all simulations confirm the feasibility of the proposed architecture, while also revealing oversizing driven by peak-current constraints, and the prototype highlights closed-loop feedback as a key direction for future work.

Key words: Lateral move irrigation, photovoltaic, PVsyst, LOGO!Soft, Simulink

Résumé

Les systèmes d'irrigation à déplacement latéral offrent une couverture efficace et uniforme des parcelles, mais leur motorisation repose généralement sur des groupes électrogènes diesel ou des câbles d'alimentation traînants, ce qui s'avère peu pratique dans des zones hors réseau comme le Sahara algérien. Cette thèse porte sur la conception et la validation d'un système d'entraînement photovoltaïque avec stockage sur batterie pour le déplacement de ces systèmes, sans inclure la fonction de pompage. La méthodologie se décline en quatre étapes : une revue de la littérature mettant en évidence l'absence de solutions d'entraînement photovoltaïque avec tampon batterie ; une approche de dimensionnement modulaire appliquée à un cas réel à Tébessa pour déterminer les besoins en puissance et les caractéristiques de la chaîne cinématique ; une validation via trois outils complémentaires (PVsyst, LOGO!Soft Comfort et MATLAB/Simulink) ; et enfin, la réalisation d'un prototype à échelle réduite basé sur Arduino, démontrant une locomotion autonome alimentée par l'énergie solaire. Les résultats de l'ensemble des simulations confirment la faisabilité de l'architecture proposée tout en révélant un surdimensionnement lié aux contraintes de courant de crête ; par ailleurs, le prototype met en évidence l'intérêt d'une régulation en boucle fermée pour les travaux futurs.

Mots-clés : Irrigation à déplacement latéral, photovoltaïque, PVsyst, LOGO!Soft, Simulink

ملخص

توفر أنظمة الري ذات الحركة الجانبية تغطية فعالة ومتجانسة لقطع الأراضي، إلا أن تشغيلها يعتمد عادةً على مولدات الديزل أو كابلات التغذية الكهربائية الممتدة، وهي حلول تفتقر إلى العملية في المناطق غير المرتبطة بالشبكة الكهربائية، مثل الصحراء الجزائرية. تتناول هذه الأطروحة تصميم والتحقق من صلاحية نظام دفع يعتمد على الطاقة الكهروضوئية مع تخزين الطاقة في بطاريات لتحريك هذه الأنظمة، وذلك دون التطرق لوظيفة الضخ. وتتوزع المنهجية المتبعة على أربع مراحل: مراجعة للأدبيات العلمية تبرز غياب حلول الدفع الكهروضوئي المزودة ببطاريات تخزين؛ واعتماد نهج لتحديد الأبعاد (التحجيم) بشكل معياري وتطبيقه على حالة واقعية في منطقة تبسة لتحديد احتياجات الطاقة وخصائص مجموعة نقل الحركة؛ والتحقق من صحة النظام عبر ثلاث أدوات برمجية متكاملة (PVsyst وLOGO!Soft Comfort وMATLAB/Simulink)؛ وأخيراً، إنجاز نموذج أولي مصغر يعتمد على منصة Arduino، مما يثبت إمكانية الحركة الذاتية للنظام اعتماداً على الطاقة الشمسية. وتؤكد نتائج جميع عمليات المحاكاة جدوى البنية المقترحة، مع الكشف عن وجود زيادة في الأبعاد (تضخيم في المواصفات) ناتجة عن متطلبات تيار الذروة؛ كما يبرز النموذج الأولي أهمية استخدام نظام تحكم ذي حلقة مغلقة (closed-loop control) في الأعمال المستقبلية.

الكلمات المفتاحية: الري ذو الحركة الجانبية، الطاقة الكهروضوئية، PVsyst، LOGO!Soft، Simulink.

Contents

General Introduction 5

I. Introduction 8

I.1 Agriculture and Irrigation Worldwide 8

I.1.1 Food security and water use 8

I.1.2 Moving sprinkler machines and irrigation efficiency 9

I.2 Agriculture and Irrigation in Algeria 9

I.2.1 Geography, climate and water resources 9

I.2.2 Agriculture, food dependence and irrigated area 10

I.2.3 The Saharan frontier 10

I.2.4 Solar resource and energy supply 10

I.3 Autonomous Irrigation Systems: Center Pivot and Lateral Move 11

I.3.1 From set-move to continuous-move machines 11

I.3.2 Center pivot machines 11

I.3.3 Lateral move machines 11

I.3.4 Center pivot and lateral move compared 12

I.3.5 Powering the movement: from cables and diesel to solar 14

I.4 Photovoltaic Panels and Lithium Batteries 15

I.4.1 Photovoltaic conversion and electrical model 15

I.4.2 Heat, dust and module choice 16

I.4.3 Power conversion and maximum power point tracking 17

I.4.4 Lithium-ion batteries 17

I.4.5 Battery management 18

I.5 Synthesis and Research Gap 18

I.5.1 What the literature establishes 18

I.5.2 The gap and the proposed architecture 19

I.6 Conclusion 19
II. Introduction 21
II.1 Proposed system functional logic 21
II.2 Modular approach 21
II.2.1 Carrying towers 21
II.2.2 Mass of the nodes 22
II.2.3 Force of rolling resistance 22
II.2.4 Required operational torque 22
II.2.5 Motor's mechanical power 22
II.3 Case study 23
II.3.1 Site choice and characteristics 23
II.3.2 Crop choice and water needs 24
II.3.3 Field requirements 24
II.3.4 Mechanical specification of the node 24
II.3.5 Drive train choice 26
II.3.6 Electrical specifications 29
II.3.7 Battery sizing 30
II.3.8 Charge regulator 31
II.3.9 PV array sizing 32
II.4 Conclusion 33
III. Introduction 35
III.1 Electrical energy needs using Pvsyst 35
III.1.1 Project type 36
III.1.2 Weather data 36
III.1.3 Orientation and tilt 37

III.1.4 Load needs 38
III.1.5 Energy conversion and storage system 38
III.1.5.1 Storage 39
III.1.5.2 The PV module 40
III.1.5.3 MPPT charge regulator 40
III.1.5.4 The PV array 40
III.1.6 Simulation results 40
III.1.6.2 Interpretation 41
III.2 PLC program using LOGO!Soft 42
III.3 System simulation using MATLAB/Simulink 45
III.3.1 System overall model 45
III.3.2 Battery block 46
III.3.3 Permanent magnet DC motor 46
III.3.4 Motor drive controller 47
III.3.5 Simulation results 47
III.3.6 Results interpretation 50
III.4 Conclusion 50
IV. Introduction 52
IV.2 System Overview 52
IV.3 Mechanical Design 53
IV.3.1 Chassis Design 53
IV.3.2 Wheels Design 53
IV.4 Power System Design 54
IV.4.1 Solar Panel Selection 54
IV.4.2 Solar Charge Controller 55

IV.4.3 Battery Selection 55
IV.5 Control System Design 56
IV.5.1 Microcontroller Selection 56
IV.5.2 Continuous Rotation Servo Motors 56
IV.5.3 On/Off Switch 57
IV.6 Circuit Design and Wiring 57
IV.8 Assembly and Final Prototype 59
IV.9 Limitations 59
IV.10 Conclusion 60
General Conclusion and perspectives 62

List of figures

Figure I.1 Coverage of a square field by a center pivot and a lateral move……13
Figure I.2 Illustrative current voltage characteristics of a generic 72-cell silicon module…….16
Figure II.1 Satellite view of the study field showing its area and perimeter (Google Earth)…….23
Figure II-2 Permanent magnet DC (PMDC) motor ……....26
Figure II-3 Speed, power and current characteristic curves of the PMDC motor as a function of torque…… 27
Figure II.4 Structure of the planetary gearbox ……..28
Figure II.5 RoboteQ MDC1460 motor driver ……..29
Figure II.6 H-bridge circuit used by the motor driver ……..29
Figure II.7 Li-Time 60A MPPT solar charge controller …… 31
Figure III.1 PVsyst photovoltaic system design and simulation software ……35
Figure III.2 Project type selection window – standalone (off-grid) system ……..36
Figure III.3 PVsyst project window showing the imported site and weather data files…….36
Figure III.4 Weather data import window – selection of the PVGIS-SARAH2 database…… 37
Figure III.5 PV array orientation and tilt optimization window ……37
Figure III.6 Definition of the system's hourly load profile (average of 7.43 Wh) …….38
Figure III.7 Battery parameters entered from the manufacturer's datasheet……...39
Figure III.8 Configuration of the battery pack …… .39
Figure III.9 Selection of the PV module in the PVsyst database ……..40
Figure III.10 Selection of the MPPT charge controller ……40
Figure III.11 Configuration of the PV array (modules per string and number of strings) …….. 40
Figure III.12 Simulation results – normalized energy production balance.……...41
Figure III.13 LOGO!Soft Comfort programming interface……...42
Figure III.14 Ladder diagram of the PLC control program ……...44
Figure III.15 Overall Simulink model of the system's power chain……...45
Figure III.16 Battery block used in the Simulink model……46
Figure III.17 Parameters of the permanent magnet DC motor block……46
Figure III.18 Motor drive controller circuit (IGBT switches and freewheeling diode)……47
Figure III.19 Simulated DC motor speed response……48
Figure III.20 Simulated DC motor torque response …….....48

Figure III.21 Simulated DC motor armature current …….....49
Figure III.22 Simulated battery output current …….....49
Figure IV.1 3D model render of the prototype…….…….....53
Figure IV.2 3D model render of the system wheels …….....54
Figure IV.3 6V 210mA solar panel …….....54
Figure IV.4 The CN3791 solar charge regulator …….....55
Figure IV.5 A 3.7 V lithium-ion battery cell …….....55
Figure IV.6 Arduino Nano …….....56
Figure IV.7 Continuous rotation servo motor MG90s …….....57
Figure IV.8 6A toggle switch …….....57
Figure IV.9 Prototype wiring schematic …….....58
Figure IV.10 A picture of the finished prototype ……..…….....59

List of Tables

Table I.1 Comparison between linear move and pivot systems 14
Table I.2 Voltage and safety characteristics of two lithium-ion chemistries (per cell) 17
Table I.3 Studies most relevant to a PV and battery powered movement drive for an irrigation machine 19
Table II.1 PMDC characteristics taken from its datasheet 27
Table II.2 Battery characteristics 31
Table II.3 Charge regulator characteristics 32
Table II.4 Solar panel characteristics 32
Table III.1 Function blocks used in the PLC program and their roles 43
Table IV.1 Connected pins on the Arduino and their function 58

List of abbreviations

PV : Photovoltaic

DC : Direct Current

PMDC : Permanent Magnet Direct Current

MPPT : Maximum Power Point Tracking

PWM : Pulse Width Modulation

PLC : Programmable Logic Controller

FBD : Function Block Diagram

LFP : Lithium Iron Phosphate

NMC : Nickel Manganese Cobalt (oxide)

BMS : Battery Management System

STC : Standard Test Conditions

SOC : State Of Charge

IGBT : Insulated Gate Bipolar Transistor

RMS : Root Mean Square

GPS : Global Positioning System

SPDT : Single Pole Double Throw

PVGIS : Photovoltaic Geographical Information System

SARAH : Surface Solar Radiation Data Set – Heliosat

MATLAB : Matrix Laboratory

USD : United States Dollar

General Introduction

General Introduction

Irrigation underpins a large share of global food production, contributing around 40% of world food output from only a fifth of cultivated land, and it remains the single largest human use of freshwater. This dependence is especially acute in Algeria, a country where renewable water resources per capita sit well below the internationally recognized scarcity threshold, and where the government has nonetheless committed to a substantial expansion of mechanized irrigation across the Sahara to reduce food import dependence. This expansion is taking place in regions where the electrical grid is weak or absent, but where solar irradiation is abundant, a combination that makes photovoltaic power an obvious, though so far underexploited, candidate for supplying the energy needs of irrigation machinery.

Among mechanized irrigation systems, the lateral move machine is particularly well suited to rectangular fields, since, unlike the center pivot, it can in principle cover the entire field area rather than leaving the corners of a square dry. This advantage in coverage and in application uniformity, however, comes at the cost of a more demanding power and guidance requirement, because a lateral move has no fixed central point, its towers cannot be powered from a single hub, so real installations rely instead on diesel generators or long trailing power cables, both of which reintroduce the fuel dependency and infrastructure cost that a remote, off-grid Saharan site can least afford.

This thesis starts from that specific, unresolved problem. Its aim is not to redesign the irrigation function of a lateral move machine, the pumping and distribution of water are explicitly left outside its scope, but to design, size, and validate an alternative power source for the machine's movement alone, using on-board photovoltaic panels and a lithium-ion battery in place of diesel or cable supply. The central question is whether such a supply can be sized reliably enough, using a general and reusable methodology, to guarantee autonomous operation under real site conditions, and whether that sizing can be confirmed both by simulation and by physical demonstration.

To answer this question, the thesis is organized into four chapters. Chapter I reviews the literature needed to situate and justify the work, moving from the global and Algerian irrigation context to the engineering of center pivot and lateral move machines and finally to photovoltaic and lithium battery technology, concluding with the identification of the specific gap this thesis addresses. Chapter II develops a modular sizing methodology, in which the machine is decomposed into

identical repeating nodes, and applies it to a real case study on a potato field in Mechta Ben Meriem, Tebessa, to obtain a fully sized mechanical, electrical, and photovoltaic solution. Chapter III validates this sizing through three complementary simulation environments PVsyst, LOGO!Soft Comfort, and MATLAB/Simulink, covering the energy balance, the control logic, and the dynamic electromechanical behavior of the system respectively. Chapter IV presents a small scale physical prototype built to demonstrate, in practice, that solar charged autonomous movement is achievable. Together, these four chapters build a complete case, from motivation to physical proof, for replacing diesel and cable power with photovoltaic and lithium battery power in lateral move irrigation systems.

Chapter I

Review of literature

I. Introduction

This thesis concerns the design of a lateral move irrigation machine whose movement, and the electrical accessories that support that movement (control, guidance and monitoring electronics), are powered by photovoltaic (PV) panels and lithium-ion batteries rather than by a diesel generator or a trailing supply cable. The scope of the work is deliberately limited to this movement load: the pumping and delivery of irrigation water are outside the thesis and are not sized, modeled or powered by the system described here. This chapter reviews the literature needed to justify and inform that design: the agronomic and water context that motivates mechanized irrigation, the engineering of autonomous moving sprinkler machines, and the photovoltaic and lithium battery technologies that can power their movement.

The chapter has five sections. Section 1.1 places irrigation in the global context of food security and water use. Section 1.2 turns to Algeria, where a dry climate, limited renewable water and an expanding Saharan irrigation frontier shape both the need for mechanized irrigation and the opportunity for solar power. Section 1.3 examines autonomous mechanized irrigation, first the center pivot and then, in greater depth, the lateral move machine, with attention to how each machine is moved and controlled. Section 1.4 reviews photovoltaic panels and lithium batteries as a power source for that movement. Section 1.5 synthesizes the findings and states the gap that this work addresses. The chapters that follow develop the operating logic, design, simulation and prototype of the machine.

I.1 Agriculture and Irrigation Worldwide

I.1.1 Food security and water use

Agriculture remains the foundation of human food supply, and the scale of the task is large. About 673 million people, or 8.2 % of the world population, experienced hunger in 2024, a slight improvement on 8.5 % in 2023 and 8.7 % in 2022, although hunger continued to rise across most of Africa [1]. Irrigation is one of the main instruments through which agricultural output is raised and stabilized: it is credited with about 40 % of world food production on roughly 20 % of the world's cropland [2]. Irrigation is also the largest human use of freshwater, accounting for more than 70 % of global withdrawals, and an estimated 3.2 billion people live in agricultural areas with high to very high water scarcity [3]. Rainfed agriculture nevertheless still covers more than 80 %

of cultivated land, so mechanized irrigation and rainfed farming are complementary rather than competing [2].

I.1.2 Moving sprinkler machines and irrigation efficiency

Three families of irrigation method are in use: surface irrigation, in which water flows over the soil by gravity; sprinkler irrigation, in which pressurized water is sprayed over the crop; and micro irrigation, in which small emitters deliver water to discrete zones [2]. Surface irrigation still dominates worldwide, covering about 85 % of the irrigated area, but sprinkler systems have grown where labor is scarce and uniform application matters [2]. Typical application efficiency ranges from about 50–80 % for surface methods to 75–95 % for the class of continuously moving sprinklers, center pivots, lateral moves and low-energy precision application systems, comparable with micro irrigation at 80–95 % [2]. Moving machines also offer high uniformity and low labor requirements, at the price of a high capital cost [2].

This combination of efficiency and low labor is why moving sprinkler machines, and in particular the lateral move examined in Section I.3, are an attractive answer to the water and labor constraints described above. The energy needed to pump the water they apply is outside the scope of this thesis; what follows instead concerns the operationally critical, energy needed to move the machine itself.

I.2 Agriculture and Irrigation in Algeria

I.2.1 Geography, climate and water resources

Algeria covers 2,381,741 km², the largest area of any African country [4]. The Sahara covers 87 % of the national territory and receives less than 100 mm of rain per year, while the coastal strip and the Tellian Atlas hold about a third of the cultivated land under an irregular Mediterranean climate [4]. Averaged over the country, rainfall is only 89 mm per year [4]. Renewable water resources amount to 11,670 million m³ per year, which for a population of about 43 million is less than 300 m³ per person per year, under 30 % of the 1,000 m³ scarcity threshold used by the World Bank [4]. Water withdrawals reached 8,425 million m³ in 2012, drawn roughly evenly from surface water and groundwater [4].

I.2.2 Agriculture, food dependence and irrigated area

Agriculture contributes about 12 % of Algerian gross domestic product, on a useful agricultural area of about 8.5 Mha in the north, in addition to some 33 Mha of pasture and rangeland [4], [5]. Domestic production does not cover demand: the agri-food trade balance shows exports of about USD 0.5 billion against imports of USD 9.4 billion, a deficit of USD 8.9 billion [5]. Reducing this food dependency has been a stated priority since 2000, pursued mainly through the extension of irrigation [5]. Irrigated area has grown accordingly, reaching about 1.43 Mha in 2019, roughly one sixth of Algerian cropland [4]. With less than 300 m^3 of renewable water available per person, every new irrigated hectare competes with domestic and industrial demand, so the efficiency of irrigation equipment is a matter of national water policy and not only of farm economics.

I.2.3 The Saharan frontier

The Sahara, long limited to oases watered by traditional surface and subsurface systems, has become the main growth area for Algerian irrigation. Since 2023 the government has committed to developing center pivots of 30 to 50 ha for cereal production over some 36,000 ha in arid Saharan regions that were traditionally irrigated by other methods, an intensification whose sustainability, in terms of groundwater use and cereal monoculture, is now the subject of active debate [6]. This expansion is by construction an energy intensive activity carried out where grid supply is weak or absent, which places the source and cost of energy, for both pumping and for moving the machines, at the center of the discussion [6]. Because circular pivots leave the corners of rectangular parcels unirrigated (Section I.3.4), it is reasonable to ask whether other machine geometries, and in particular the lateral move, could suit some Saharan parcels better; the sources reviewed for this thesis contain no data on lateral move deployment in Algeria, which is itself a finding.

I.2.4 Solar resource and energy supply

Algeria is well placed to replace diesel with solar power. About 3,000 hours of sunshine per year on average, and a global horizontal irradiation of almost 1,700 kWh/m^2 per year in the north rising to 2,263 kWh/m^2 per year in the south, are reported for the country, although installed solar capacity remained only 437 MW at the end of 2023 [7]. This resource has already motivated research on photovoltaic powered pumping for Algerian irrigation; the present work instead addresses the

distinct load of moving the machine itself, using photovoltaic panels and lithium batteries, which Section I.4 discusses.

I.3 Autonomous Irrigation Systems: Center Pivot and Lateral Move

I.3.1 From set-move to continuous-move machines

Sprinkler systems are classed as solid set, in which pipe and sprinklers are permanently laid out; set-move, in which lines are relocated by hand or engine between irrigations; and moving systems, which apply water while traveling continuously [2]. The last group, comprising center pivots, lateral (linear) moves and traveling guns, replaced manual relocation with continuous, self-propelled motion [2]. That step is usually traced to a self-propelled sprinkler prototype built in 1948 and put into commercial production a few years later [8]. By 2008, center pivots served 45 % of irrigated land in the United States, an increase of 124 % since 1988 [2]. The lateral move machine is a direct descendant: it is built in the same way, with towers carrying spans of pipe, but all towers travel at the same speed and in the same direction instead of rotating around a fixed point [2].

I.3.2 Center pivot machines

A center pivot consists of a fixed pivot structure that supplies water and power, and a line of spans, typically 30–65 m long, carried by A-frame towers that hold the pipe 2–4 m above the ground, each driven by an electric or hydraulic motor [2]. A typical machine has eight spans, a length of about 400 m and irrigates 50–60 ha [2]. Towers are driven sequentially and kept aligned by switches, and the average travel speed is set by the on-time of the outermost tower [2]. Two features of the geometry matter for what follows. First, the water application rate must increase with distance from the pivot, because outer spans cover much more ground per revolution than inner ones [2]. Second, a circle does not fill a square or rectangular field, so the corners are difficult to irrigate [9].

I.3.3 Lateral move machines

A lateral move irrigator has the same structural components as a pivot: a water carrying pipe supported by spans and towers, drop tubes with sprinklers, and a drive motor with a gearbox on each tower What differs is the motion and the way water and power are delivered. A control unit at one end moves the towers in a straight line so as to irrigate a rectangular field; water usually

arrives through a drag hose connected to a buried or surface main, or in ditch fed machines, through an on-board pump drawing from an open ditch that runs parallel to the direction of travel [2]. Because the drag hose is limited to about 150 m, a hose-fed machine can travel about 300 m before it must be reconnected to the next riser [2]. Commercial hose-fed laterals serve fields of roughly 32 to 130 ha; two-wheel towers cover field widths up to about 400 m and four-wheel towers up to about 790 m, with drag hoses of 219–280 m [10].

Power for the drive motors has conventionally come from an on-board diesel generator or from a trailing electrical cable, because supplying numerous tower motors from a fixed point becomes difficult once the machine is long, and because cable repair over such a distance is costly [11]. This dependence on fossil fuel or on a cable is exactly what a PV and battery supply is intended to remove, and is discussed further in Section I.4.

A lateral move also needs guidance, which a pivot does not. Because the machine is long, a small angular error at one tower produces a large displacement at the far end, and a boom that drifts can leave the field and damage fences or structures; systems that only keep the boom straight cannot correct such drift, because the whole boom may turn while remaining straight [9]. Guidance references described in the patent literature and in current products include a buried wire, an above-ground cable, a furrow and GPS [9], [10]. Towers are kept aligned by switches in the same way as on a pivot, and travel speed is commonly set by a percentage timer that energizes the drive motors intermittently, so that the average drive power is approximately the product of the duty ratio and the rated motor power [2].

A pivoting lateral variant can turn at the end of a field and so handle irregular or L-shaped fields, and the manufacturer states that this variant needs lower water pressure and causes less wear than a purely straight line machine [10]. Manufacturer literature also claims coverage of up to 98 % for fields of up to 130 ha and water savings of 50–70 % compared with furrow irrigation [10]; these are marketing statements and have not been verified independently, but their direction is consistent with the efficiency ranges of Section 1.1.2.

I.3.4 Center pivot and lateral move compared

The most visible difference is the shape of the irrigated area. A circle inscribed in a square covers $\pi/4$, or 78.5 %, of the square (Figure I.1); a lateral move whose length matches the field's width can in principle cover the whole rectangle. A second difference concerns uniformity along the

machine: on a lateral move all towers move at the same speed, so the application rate does not need to increase along the boom as it must on a pivot [2]. The price paid is guidance, the management of the hose or cable, and a higher capital cost per hectare that in practice restricts the lateral move to high value crops [11].

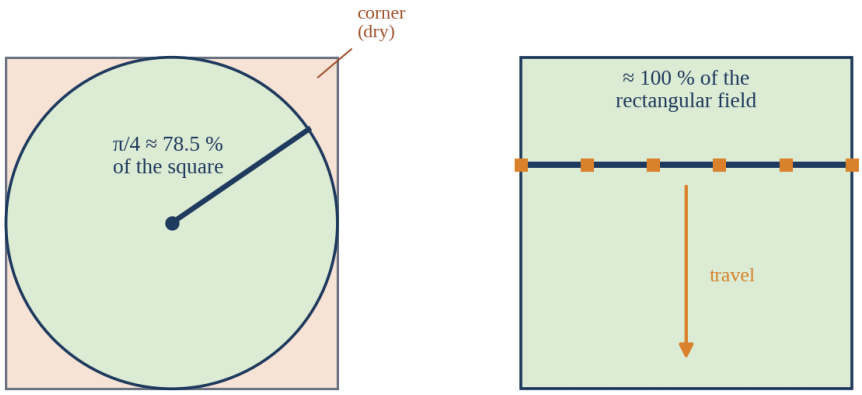


Figure I.-1 Coverage of a square field by a center pivot and of a rectangular field by a lateral move

In the Table I.1 we have listed the major characteristics of both the lateral move and centre pivot systems to better differentiate between the two systems.

Table I 1 comparison between linear move and pivot systems

Characteristic	Center pivot	Lateral move
Path of motion	Circle around a fixed pivot point	Straight line perpendicular to the pipe [9]
Field shape	Circular; corners of square fields are difficult to irrigate [9]	Square or rectangular; L-shaped with a pivoting variant [10]
Coverage of a square field	$\pi/4 \approx 78.5$ % (calculated)	Up to 98 % (manufacturer claim) [10]
Water and power supply	Through the fixed pivot point [2]	Drag hose or cable, or on board pump and generator [2]
Application rate along the machine	Increases with distance from the pivot [2]	Uniform, since all towers move at the same speed [2]
Guidance	Not needed beyond span alignment	Required: cable, furrow, GPS [9], [10]
Typical use	Very widespread, low labor [2]	High-value crops, higher capital cost [11]

I.3.5 Powering the movement: from cables and diesel to solar

Experimental evidence exists for the case of a PV powered center pivot. Herraiz et al. monitored, for three years, an installation in Spain in which a battery-free PV system supplied, among other loads, the drive motors of several pivots; those motors were driven by a dedicated frequency converter run at a constant 50 Hz and consumed 4.5 kW on average, with current peaks at start and stop [12]. The system operated without batteries, and its authors noted that sudden irradiance changes can cause control instabilities in large PV powered installations [12]. A smaller, laboratory-scale test of a pivot fed directly by PV panels without any storage found unstable power generation and recommended a battery bank to stabilize the supply to the machine [13]. Together, these two studies indicate that the energy needed to move an irrigation machine is of a manageable scale for a PV supply, but that direct, unbuffered coupling is unstable and that battery storage is the remedy proposed by the authors who observed the instability.

A local precedent exists in Algeria. A Master's dissertation at the University of Blida 1 sized a battery-backed PV supply for two 1 hp (750 W) motors, 1.5 kW in total, that move two spans of a pivot at El Menia. With 380 W modules and a 50 % discharge limit for lead–acid batteries, the calculation gave 16 modules, four for the motors, eight for battery charging to allow night irrigation and four to cover losses, whereas 18 modules were found installed on the farm, a slight oversizing that the authors discuss [14]. This dissertation is, among the sources reviewed, the closest local precedent for the system considered in this thesis, although it addresses a pivot rather than a lateral move, and uses lead–acid rather than lithium storage.

I.4 Photovoltaic Panels and Lithium Batteries

I.4.1 Photovoltaic conversion and electrical model

A PV cell is a semiconductor p–n junction: photons with energy above the band gap create electron–hole pairs that the electric field of the junction separates, producing a photocurrent [15]. Cells are connected in series to raise the voltage, and modules are connected in series and parallel to form arrays [15]. The most widely used electrical model of a cell or module is the single-diode model with series and shunt resistances [15]:

$$I = I_{ph} - I_0 \left[\exp\left((V + I R_s) / (n N_s V_t)\right) - 1\right] - (V + I R_s) / R_{sh} \qquad \text{(I.1)}$$

where I and V are the terminal current and voltage, I_{ph} the photocurrent, I_0 the diode saturation current, n the ideality factor, N_s the number of cells in series, $V_t = kT/q$ the thermal voltage, and R_s and R_{sh} the series and shunt resistances. The photocurrent is approximately proportional to irradiance, so short-circuit current scales linearly with it, whereas open-circuit voltage falls as temperature rises; the maximum power point therefore moves with both variables (Figure I.2).

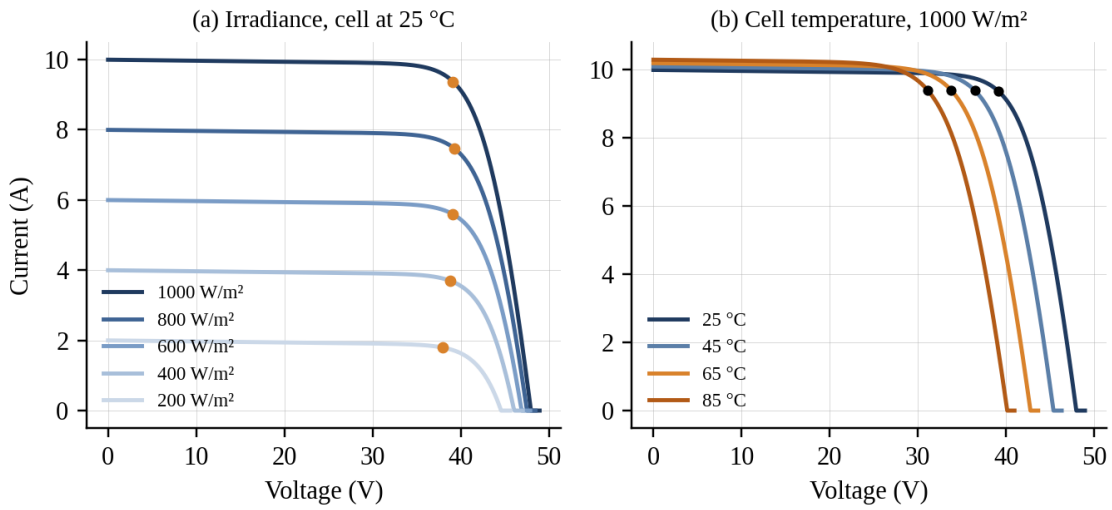


Figure I-2. Illustrative current–voltage characteristics of a generic 72-cell silicon module

Around the maximum power point, the output can be expressed approximately as a function of irradiance G and cell temperature T_c [15]:

$$P_{mp} = P_{STC}\,(G / 1000)\,[1 + \gamma\,(T_c - 25)] \qquad \text{(I.2)}$$

where P_{STC} is the rated power under standard test conditions and γ is the temperature coefficient of power, negative for silicon and typically around −0.3 to −0.4 %/°C for commercial modules. In hot conditions, cell temperatures 40–50 °C above ambient are plausible, which such a coefficient translates into a power loss on the order of 15–20 % relative to standard test conditions, a loss that module choice and mounting can only partly mitigate.

I.4.2 Heat, dust and module choice

Two environmental factors dominate PV performance in the Algerian south. The first is heat, quantified above through Eq. (I.2). The second is dust: measurements in Adrar found that sandstorms and dust accumulation reduce module power because of decreased glass transmittance, and that partial cleaning can itself introduce shading and mismatch losses [16]. Cleaning is therefore a design variable and not a maintenance detail for a Saharan installation. For a machine mounted array, module selection should also weigh power per unit area and mass.

I.4.3 Power conversion and maximum power point tracking

Between the array and the load, a DC–DC converter under maximum power point tracking (MPPT) adjusts the operating point so the array delivers its maximum available power as irradiance and temperature vary; Esram and Chapman found at least 19 distinct MPPT methods in the literature, of which perturb-and-observe and incremental-conductance are the most widely applied [17]. Intermittency from passing clouds is the main practical difficulty: it can destabilize converters supplying a motor load, as the instability observed on a directly-coupled pivot drive illustrates [12], [13]. A battery on the DC bus decouples the instantaneous PV power from the motor power, so that the drives see a stable supply; this is the role storage plays in the architecture proposed in Section I.5.

I.4.4 Lithium-ion batteries

Lithium-ion is a family of chemistries that share an operating principle, the shuttling of lithium ions between electrodes, but differ in cathode material and therefore in voltage, energy density, life and safety [18]. Lithium nickel manganese cobalt oxide (NMC) delivers a higher specific energy, 150–220 Wh/kg, than lithium iron phosphate (LFP), 90–120 Wh/kg, but LFP has a higher thermal-runaway onset temperature, about 270 °C against about 210 °C for NMC, and a flat discharge voltage curve. Major differences are listed in the Table I.2 below [18].

Table I 2 . Voltage and safety characteristics of two lithium-ion chemistries (per cell).

Chemistry	Nominal voltage (V)	Full-charge voltage (V)	Runaway onset	Specific energy
NMC (nickel manganese cobalt oxide)	3.60–3.70	4.20	≈ 210 °C	150–220 Wh/kg
LFP (lithium iron phosphate)	3.20–3.30	3.65	≈ 270 °C	90–120 Wh/kg

For a slow-moving machine that is exposed to sun and dust and may be maintained far from a service center, the properties of LFP that matter most are safety, tolerance of full charge, cycle life and cost; its lower gravimetric energy is a smaller disadvantage than in a vehicle, because the battery is a small part of the mass of a water-filled steel structure, a judgment to be checked against the design. Series strings of LFP cells give convenient bus voltages: 16 cells in series give a nominal 51.2 V (16 × 3.2 V), a charge limit of 58.4 V and a discharge floor of 40 V, using the cell values of Table I.2.

I.4.5 Battery management

A battery management system (BMS) is indispensable for a lithium-ion pack. Its functions include monitoring cell voltage, current and temperature; protecting against overcharge, over-discharge, overcurrent and over-temperature; balancing the cells; and estimating the state of charge (SOC), which indicates the energy remaining and guides charging and discharging decisions [19]. Accurate SOC estimation remains difficult because of complex electrochemical behavior and aging, and the flat discharge-voltage curve of LFP noted above means that voltage alone is a poor indicator of charge over most of the usable range, which strengthens the case for a well-calibrated current sensor and periodic recalibration [18], [19].

I.5 Synthesis and Research Gap

I.5.1 What the literature establishes

Three conclusions can be drawn from the review. First, the need is real: Algeria combines less than 300 m³ of renewable water per inhabitant [4] with a large food import bill [5] and a policy of extending irrigation into the Sahara, an activity that is energy-intensive and depends on diesel where the grid is weak [6]. Second, moving sprinkler machines are the accepted answer to the demand for uniform, labor-saving irrigation [2], and the lateral move in particular covers a rectangular field more completely than a pivot, at the price of guidance and of a more demanding power supply [9], [11]. Third, the technologies needed to remove that dependence on diesel or cable are available and have been partially demonstrated: photovoltaic drive power has been shown to be of a manageable scale on a pivot [12], direct coupling without storage is unstable [13], and a local precedent exists for sizing PV and batteries to move pivot spans, using lead acid storage [14]. Lithium iron phosphate batteries and a proper BMS address the safety and durability that lead–acid storage lacks [18], [19]. Table I.3 summarizes the studies most relevant to this thesis.

Table I 3 Studies most relevant to a PV and battery powered movement drive for an irrigation machine.

Study	System	Energy architecture	Relation to this work
Herraiz *et al.* [12]	Pivot drive motors, 88 ha, Spain	Battery-free PV; dedicated frequency converter	Shows drive power is of a manageable scale; no storage used
Berwanger *et al.* [13]	Laboratory-scale pivot, direct PV coupling	No storage	Confirms the need for a buffering battery
Yantren and Bouzouidja [14]	Pivot spans, El Menia, Algeria	PV with lead–acid battery	Closest local precedent; lead–acid, pivot geometry

I.5.2 The gap and the proposed architecture

Within the sources reviewed, no work presents a lateral move machine whose movement is powered by on-board photovoltaic panels and lithium batteries, together with a design methodology and a validated model. The related evidence is of two kinds: experiments on pivots that identify the instability of unbuffered PV supply and the practicable scale of drive power [12], [13]; and a local dissertation that sizes lead–acid storage for a pivot [14]. Nothing in the literature addresses the specific combination of a straight line machine, whose guidance and alignment must be maintained under a variable energy supply, with lithium iron phosphate storage.

The concept examined in this thesis is a power path in which PV modules feed a DC bus through MPPT converters, a lithium battery with a BMS buffers the bus, and motor drives energize the tower motors under a supervisory controller. Water supply and pumping are outside this power path and are not addressed by the system.

I.6 Conclusion

This chapter has shown that irrigation is central to food production and freshwater use worldwide, that Algeria is expanding energy intensive irrigation in a region of strong solar resource, that the lateral move is an efficient and geometrically well adapted machine whose movement still typically relies on diesel or a cable, and that PV and lithium battery technologies are mature enough to power that movement instead, provided heat, dust, intermittency and battery management are addressed. The next chapter develops the operating logic of the proposed machine and a case study.

Chapter II : Theoretical approach And a Case study

II. Introduction

This chapter presents the design methodology of the solar-powered linear-move irrigation system studied in this work. It is organized in three main parts. The first part, Proposed system functional logic, establishes the general operating principle of the system and a flowchart to better visualize this logic. The second part introduces the modular approach adopted to size the system, in which the system is decomposed into identical repeating units so that the power and energy requirements of a single unit can be determined and then extended to the rest of the system. The third part applies this methodology to a case study on a real agricultural site, covering the site and crop characteristics, the resulting field layout, and the mechanical, electrical and photovoltaic sizing of the node. The chapter closes with a conclusion summarizing the main results obtained.

II.1 Proposed system functional logic

In the operating mode, the system moves sequentially by distances determined by the sprinkler range, with these movements interspersed by pauses lasting according to irrigation needs. After covering the length of the field, the system reverses direction and goes back to the starting point to repeats the same sequence. Furthermore, the duration of the pauses is significant relative to the movement time, this allows the system to use energy from storage batteries to power the electric motors while moving, and then to recharge those same batteries during the pauses.

II.2 Modular approach

Instead of looking at the system as a single continuous unit we have divided it into modular units where it can be scaled based on the crop field needs. This way we can determine the power requirements for a single unit and copy it throughout the rest of the system.

II.2.1 Carrying towers

Since the system is mainly composed of pipe sections and carrying towers, the number of towers is defined as follows :

$$N_t = \frac{L_{pipe}}{L_{section}} + 1 \qquad \text{(II.1)}$$

We have two types of towers, the end towers which carry their weight plus half the weight of their pipe section. And intermediate towers which carry their own weight plus the weight of a full pipe section. All towers are identical except the first and main tower which houses also the PLC unit. Hence we shall take the intermediate towers as the nodes because they are the worst case scenario in regards to power needs.

II.2.2 Mass of the nodes

The mass of a single node is composed of the following :

- Mass of the empty pipe and its supporting frame
- Mass of the water inside the pipe
- Mass of the tower's frame
- Mass of the wheels
- Mass of the electrical components

$$M_{node} = M_{pipe} + M_{water} + M_{tower} + M_{wheels} + M_{components} \quad \text{(II.2)}$$

II.2.3 Force of rolling resistance

The force of rolling resistance F_{rr} is the resistance of the soil to the movement of the wheels and its characterized by its coefficient C_{rr}. Wherein the coefficient of rolling resistance defines the interaction between the rubber tires and the soil, for our case of tractor type rubber tires on wet soil the coefficient range is [0.1 ; 0.2], we will assume a value of $C_{rr} = 0.15$ [20]

$$F_{rr} = M_{node} \times g \times C_{rr} \quad \text{(II.3)}$$

II.2.4 Required operational torque

The torque required T_r is the force of rolling resistance multiplied by the wheel's radius R_{wheel}

$$T_r = F_{rr} \times R_{wheel} \quad \text{(II.4)}$$

II.2.5 Motor's mechanical power

Since there is a single motor in each node driving both wheels, its required mechanical power P_{mec} is the required torque T_r multiplied by the angular velocity of the wheel Ω_{wheel} in rad/s and divided by the efficiency of the gearbox η_g.

$$P_{mec} = \frac{T_r \times \Omega_{wheel}}{\eta_g} \quad \text{(II.5)}$$

II.3 Case study

Having established the theoretical model and the modular approach used to size a single node, this section applies that methodology to a real site. We present the chosen location, the crop and its water needs, and the resulting field layout, before sizing the mechanical, electrical and photovoltaic components of the node accordingly.

II.3.1 Site choice and characteristics

The chosen site for the following study, represented by a satellite view image in Figure II.1 is known as Mechta Ben Meriem located in the municipality of El Huidjbet wilaya de Tebessa at the coordinates [35.280959°, 008.245883°]. This region, positioned in the northern edge of the Sahara Desert, benefits from an exceptionally favorable solar climate characterized by high direct normal irradiance throughout the year with an annual average of 1956.3 kWh/m^2. while the daily normal irradiance average is around 225Wh/m^2 [21].

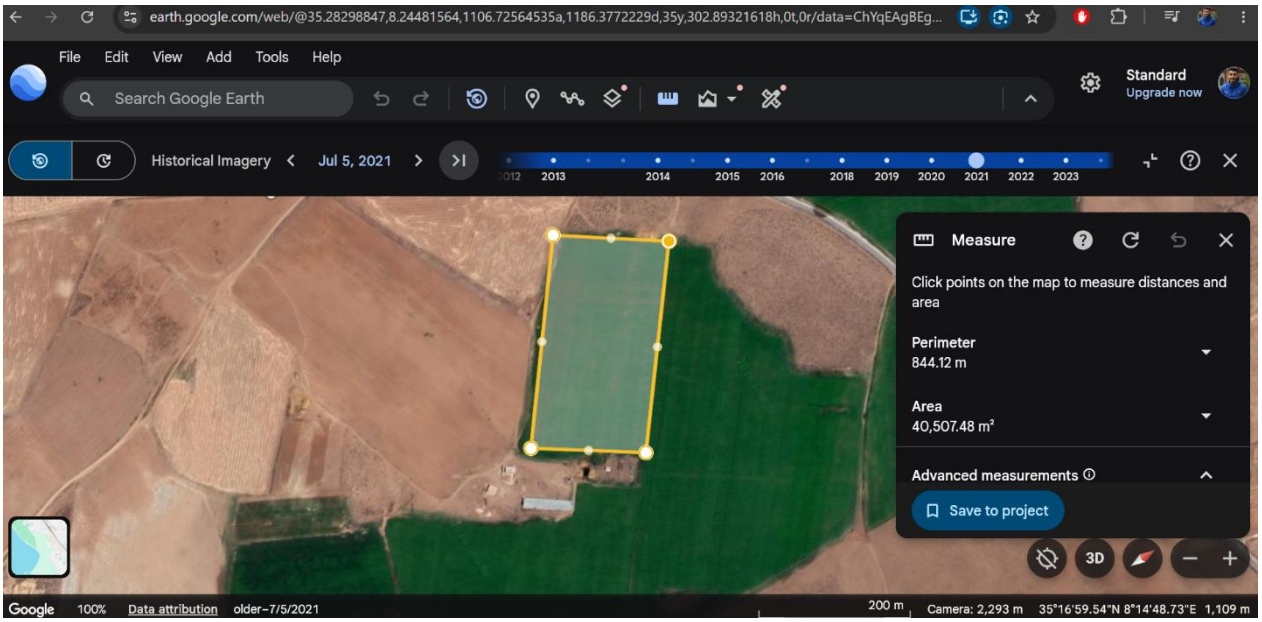


Figure II.1 Satellite view of the study field showing its area and perimeter (Google Earth)

This location ensures minimal cloud cover and extended daylight hours, making it an optimal choice for photovoltaic based system deployment. The area of the intended field is 40500 m^2 with a length of 270m and a width of 150m.

II.3.2 Crop choice and water needs

The chosen crop for this study is potatoes, because it was already cultivated many times before in this land, also the soil type is sandy which makes it a very good candidate for vegetables that grow underground and require space to develop.

Water needs for potatoes are heavily dependent on the soil type and meteorological situation but based on the cultivation that have been executed in previous years, it have been established that the water needs are supplied in 3 hours intervals every 3 days, using a pipe of 75mm in diameter to supply the water to the double ended sprinklers with a water pressure of 400kpa, the sprinklers have a reach of 12m. these parameters serve the purpose of maintaining a water penetration rate of around 6mm.

II.3.3 Field requirements

Following the modular approach established earlier we will start by choosing a pipe line length of 150m to fill the width of the field, with a pipe section length of 50m. which gives us 4 carrying towers based on equation (II.1).

Based on the field length of 270m, the sprinklers reach of 12m and the irrigation interval of 3hours. The system will cover the whole field in 69 hours with 23 stops. So we can choose a slow travel speed of 1.8km/h.

II.3.4 Mechanical specification of the node

We shall start by determining the mass of node's components :

The mass of the main pipe : [22]

$$M_{pipe} = 5.32\ {}^{kg}/_{m}$$

Which gives us a full mass of

$$M_{pipe} = 266\ kg$$

Mass of the water in the pipe :

We calculate first the volume of the water in the pipe V_{water}

$$V_{water} = \pi \times {R_{pipe}}^2 \times L_{section} \quad \text{(II.6)}$$

$$V_{water} = \pi \times 0.0375^2 \times 50$$

$$V_{water} = 220\ L$$

So the mass of the water equals :

$$M_{water} = V_{water} \times \rho \quad \text{(II.7)}$$

$$M_{water} = 220 \times 1000$$

$$M_{water} = 220\ kg$$

Mass of the tower :

We have estimated the number of structural steel bars and sheets and their combined mass was equal to [22]

$$M_{tower} = 75\ kg$$

Mass of the wheels :

We have two 1.2m diameter wheels per tower with each wheel weighing $100\ kg$ so their total mass is [23]

$$M_{wheels} = 200\ kg$$

Mass of the components :

We cannot determine the exact mass of all the electrical components in each node, so we have decided to represent it as a 20% mass increase over the total mass of the node.

$$M_{components} = M_{node} \times 0.2 \quad \text{(II.8)}$$

Mass of the node :

$$M_{node} = M_{pipe} + M_{water} + M_{tower} + M_{wheels} + M_{components}$$

$$M_{node} = 915kg$$

After establishing the mass of the node we can do the numerical application on equations (II.3) and (II.4). Which gives us

$$F_{rr} = 1346.5\ N$$

$$T_r = 807\ N.m$$

To determine the nominal required mechanical power to move the node we must first differentiate between its different phases of motion, which there are two :

The transitional phase is where the system starts from a full stop and gets up to speed. This phase is characterized by a high startup torque which is around 2 to 3 times the steady state rolling resistance torque. This multiplier was adopted to account for soil deformation, wheel sinkage, and transient traction effects, and it should be covered by the startup torque of the driving motor.

The steady motion phase is where the system is already moving at a constant speed of 1.8 km/h and it's the base line for our nominal required mechanical power calculations.

Motor's mechanical power :

Since the system's chosen speed is 1.8km/h, this gives an angular velocity of the wheels of 0.837rad/s and using a planetary gearbox with an efficiency of 98% we can determine the motor's mechanical power output using equation (II.5)

$$P_{mec} = 711W$$

II.3.5 Drive train choice

The PMDC motor :

To provide this power we have chosen a permanent magnet DC motor from Leeson, the exact motor is shown in Figure II.2 below. [24]



Figure II.2 Leeson permanent magnet DC motor[24]

The choice of this exact motor was based on the calculations made previously and based on the motor's specifications shown in Table II.1 below.

Table II 1 PMDC motor characteristics taken from its datasheet[24]

Specification	Value
Nominal output power P_n	750 W
Absorbed power	915 W
Nominal speed N_n	1800 rpm
Efficiency at full load η	82%
nominal current I_n	18.5A
Nominal voltage V_n	48 V
Nominal torque T_n	3.95 N.m
maximum current I_s	165 A
Stall torque T_{stall}	350 N.m

The second major factor for selecting this specific motor is it's characteristics curves mainly the Speed, power and current curves shown in the Figure II.3 below.

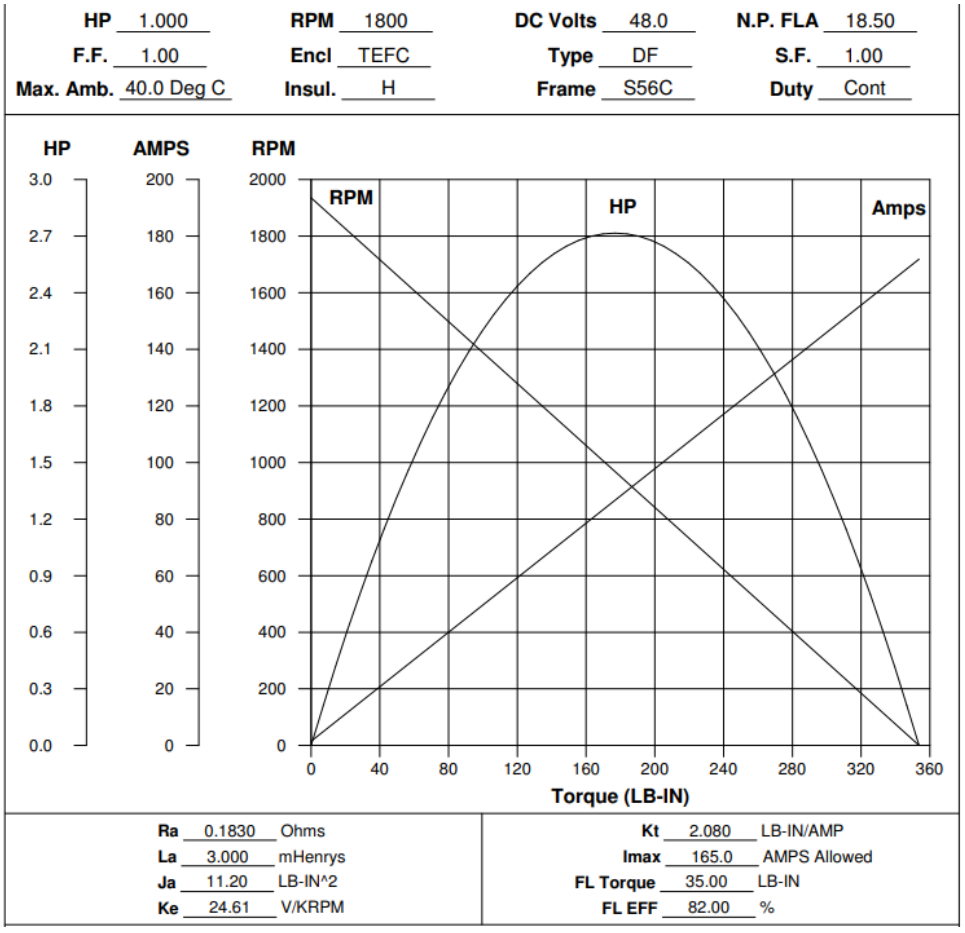


Figure II-3 Speed, power and current characteristic curves of the PMDC motor as a function of torque[24]

Based on the characteristics of this motor presented above, the reasons why it was selected for this system are the following :

- The linear speed torque characteristic of the PMDC motors which lets the motor retain its speed whatever the load torque is.
- Removing the need for an inverter between the battery and the machine.
- The straightforward speed control which require only varying the voltage source using a PWM DC-DC converter.

The gear box :

Running the motor using a PWM converter at a speed of 8rpm is impractical due to the cogging phenomenon. This forces us to reduce the speed of the motor to 500rpm electrically then pairing that output with a gearbox with a reduction ratio of 62:1 to achieve the necessary output speed at the wheels. A planetary gearbox was chosen for to its high efficiency and compact design, it's constituents are presented in the Figure II.4 below. [25]

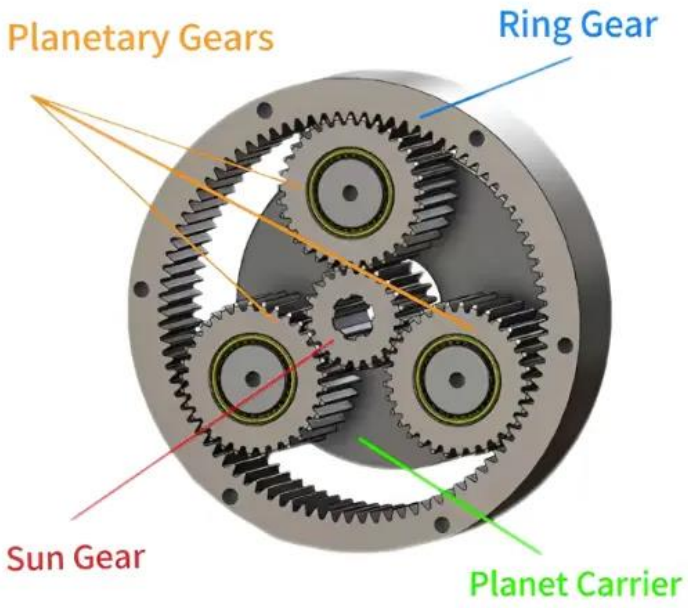


Figure II.4 : Structure of the planetary gearbox

The motor driver :

The chosen driver for this task is MDC1460 presented in Figure II.5 below. This is a four-quadrant DC motor controller (H-bridge driver). It uses PWM to control the motor's input voltage and therefore its speed. This particular controller can be used in open loop configuration with no feedback from the motor. Or in a closed loop configuration which makes it able to respond to

variations in speed or current. It serves two major functions, the first is limiting the startup current so the motor does not burn itself, and the second function is control the speed of the motor reducing it to 500rpm by acting on the input voltage.[26]



Figure II.5 : RoboteQ MDC1460 motor driver[26]

In the Figure II.6 below is the equivalent electric circuit of the four quadrant DC-DC converter which consists of 4 controlled switches and four freewheeling diodes.

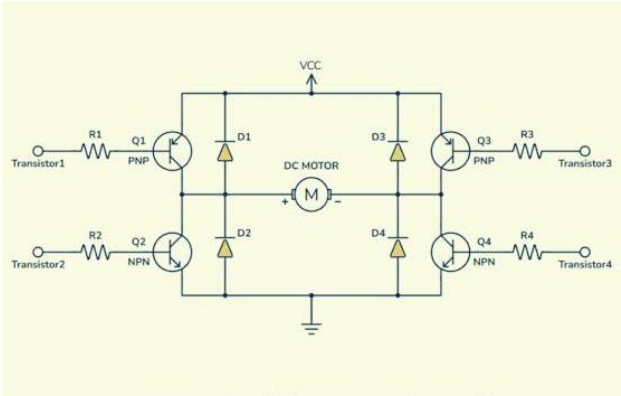


Figure II.6 : H-bridge circuit used by the motor driver

II.3.6 Electrical specifications

After choosing the drivetrain for the system we must determine its power and energy consumption to size the battery and solar panels accordingly.

We have chosen a battery capacity autonomy of 3 days which is enough for a full irrigation cycle of the proposed field.

Motor's energy consumption

The system have to cover the field's length of 270m twice every 3 days at a constant speed of 1.8km/h which gives a motor running time t_m of :

$$t_m = 2 \times \frac{0.27}{1.8} \quad \text{(II.9)}$$

$$t_m = 0.3\ hour$$

This running time translates to a motor energy consumption E_m of :

$$E_m = P_{ab} \times t_m \quad \text{(II.10)}$$

$$E_m = 275\ Wh$$

Controller energy consumption :

The controller idle power consumption is rated at 3.6 watts, during the three days cycle this gives us an energy consumption $E_{controller}$ [26]

$$E_{controller} = 260Wh$$

Total energy consumption :

The total energy E_{total} is the sum of energies consumed by the electrical equipment of the system

$$E_{total} = E_{controller} + E_m \quad \text{(II.11)}$$

$$E_{total} = 535\ Wh$$

II.3.7 Battery sizing

Although we have established the total energy requirements of the system for the chosen battery's capacity autonomy, it is not the single determining factor in this case. The battery must also be able to support the high current draw of the motor during operation.

To determine this current I we must find the motor's output torque T_{out} at the speed of 500rpm which corresponds to the torque at the wheels T_{wheel} divided by the gear ratio

$$T_{out} = \frac{T_{wheel}}{62} \quad \text{(II.12)}$$

$$T_{out} = 13.06\ Nm$$

Which corresponds from the graph in figure II.4 to a current draw of 53A

Based on this calculations we picked a 48V 15Ah LiFePO4 battery, its specifications are presented in the Table II.2 below. [27]

Table II 2 battery characteristics[27]

Specification	Value
Battery rated voltage	48V
Battery rated capacity	15Ah
Max discharge current	60A
Cycle life	2500 cycles
Charging current	3A

II.3.8 Charge regulator

The role of the charging regulator is as its name indicates, takes the input power of the solar array and regulates the voltage and current to charge the battery, while using a maximum power point tracking algorithm (MPPT) to maximize the power obtained from the solar array.

The chosen regulator is Li-Time 60A MPPT solar charge controller, (Figure II.7)



Figure II.7 : Li-Time 60A MPPT solar charge controller [28]

This Charge controller is characterized by the specifications shown in Table II.3 below.

Table II 3 charge regulator characteristics[28]

Specification	Value
Battery voltage	9V to 64V
Max solar input voltage	150V
MPPT voltage range	3V to 120V
Max input power	3200W
Max charging current	60A

II.3.9 PV array sizing

Solar panel choice :

For the solar panel we have decided to use the Jinkosolar JKM-240M solar panel which has the following specifications mentioned in the Table II.4 below. [29]

Table II 4 solar panel characteristics [29]

Specification	Value
Technology	Monocrystalline
Max power	240 Wp
Max voltage	48 V
Max current	5.05 A
Open circuit voltage	57.6 V
Short circuit current	5.66 A
Number of cells	96 cells
Module size	1.7 m^2
Module efficiency at 25 C° η_{PV}	14%

The choice of this solar panel was made in correspondence to the solar charger requirements specified earlier, mainly its input voltage and current ranges.

In the worst case scenario where there is minimal solar irradiance of 225W/m^2, and our total modules surface is 1.7 m^2, we will be receiving an effective irradiance of G_{eff} of

$$G_{eff} = 225 \times 1.7$$

$$G_{eff} = 382.5\ W/m^2$$

This effective irradiance is then converted to an electrical power by the PV array with a power of

$$P_{min} = G_{eff} \times \eta_{PV} \quad \text{(II.13)}$$

$$P_{min} = 53.55W$$

This minimum energy can fully charge the 15Ah battery pack from 0% in a duration t_{ch} of

$$t_{ch} = \frac{V_B \times 15}{P_{min}} \quad \text{(II.14)}$$

$$t_{ch} = \frac{48 \times 15}{53.55}$$

$$t_{ch} = 13.5 \text{ h}$$

This charging time is very good compared to the battery full discharge duration of 72 hours

II.4 Conclusion

This chapter set out to define a standard methodology for evaluating the power needs of a linear-move irrigation system. By decomposing the system into identical modular nodes, each carrying its own tower, pipe section and drivetrain, we were able to derive a compact set of equations covering the mechanical load, the required torque and the resulting mechanical and electrical power demand of a single unit, independently of the overall length of the system.

Applying this methodology to the case study of a 270 m by 150 m potato field in Mechta Ben Meriem allowed every stage of the design to be sized consistently: the number and mass of the carrying towers, the required motor torque and power, the choice of a permanent magnet DC motor with a planetary gearbox and its driver, and finally the battery and photovoltaic array needed to supply the system autonomously. The resulting 48V 15Ah LiFePO4 battery and 240 Wp solar panel were shown to comfortably cover the energy and current requirements of the drivetrain, even under the site's worst-case irradiance conditions, confirming the feasibility of a fully solar-powered node. This validated sizing approach provides the basis for the experimental and simulation work presented in the following chapter.

Chapter III : System simulation using PVsyst, LogoSoft! and Matlab/Simulink

III. Introduction

This chapter is dedicated to the simulation of the different subsystems that make up the proposed solar-powered irrigation system, as well as the interactions between them. Three complementary simulation environments are used, each addressing a specific aspect of the system. PVsyst is used to simulate the electrical energy needs and to evaluate the performance of the photovoltaic generation and storage chain. LOGO!Soft Comfort is used to design, program and simulate the programmable logic controller (PLC) responsible for the automatic control of the system. Finally, MATLAB/Simulink is used to simulate the overall power chain of the system, from the battery to the DC motor, under real operating conditions, in order to validate the sizing choices made in the previous chapter. The results obtained from each of these three simulation tools are presented and discussed throughout this chapter.

III.1 Electrical energy needs using Pvsyst

PVsyst (Figure III.1) is a specialized software application widely used for the design, simulation, and performance analysis of photovoltaic (PV) systems. Developed specifically for solar energy projects, it enables engineers, researchers, and project developers to evaluate the energy production, efficiency, and economic feasibility of grid-connected, off-grid, and pumping systems. By incorporating detailed meteorological data, system components, shading analysis, and loss calculations, PVsyst helps optimize solar installations and predict their long-term performance with a high degree of accuracy. Using this software to run a simulation for our photovoltaic system we must follow the next steps.



Figure III.1: PVsyst photovoltaic system design and simulation software

III.1.1 Project type

The first step is to choose the project's type (Figure III.2). Our system is fully autonomous and off-grid so we pick the standalone project.

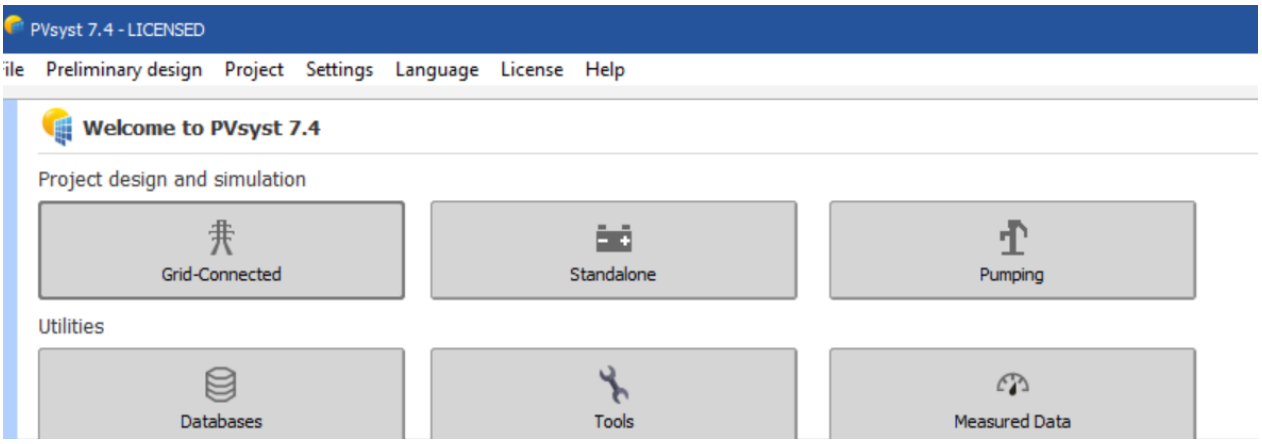


Figure III.2: Project type selection window – standalone (off-grid) system.

III.1.2 Weather data

The next step is selecting our site location and importing meteorological data from the different databases available (Figure III.3).

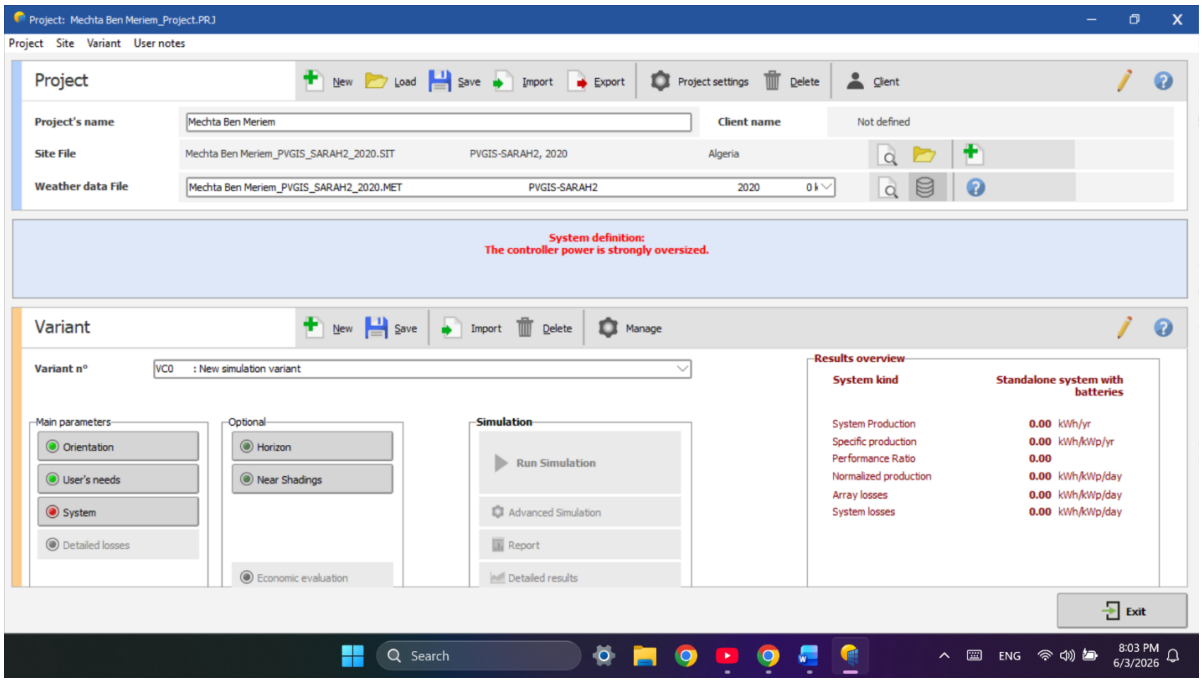


Figure III.3 PVsyst project window showing the imported site and weather data files

We chose to import the hourly meteorological data from the PVGIS_SARAH2 data base since it is the one providing the most recent and accurate data from the different databases (Figure III.4).

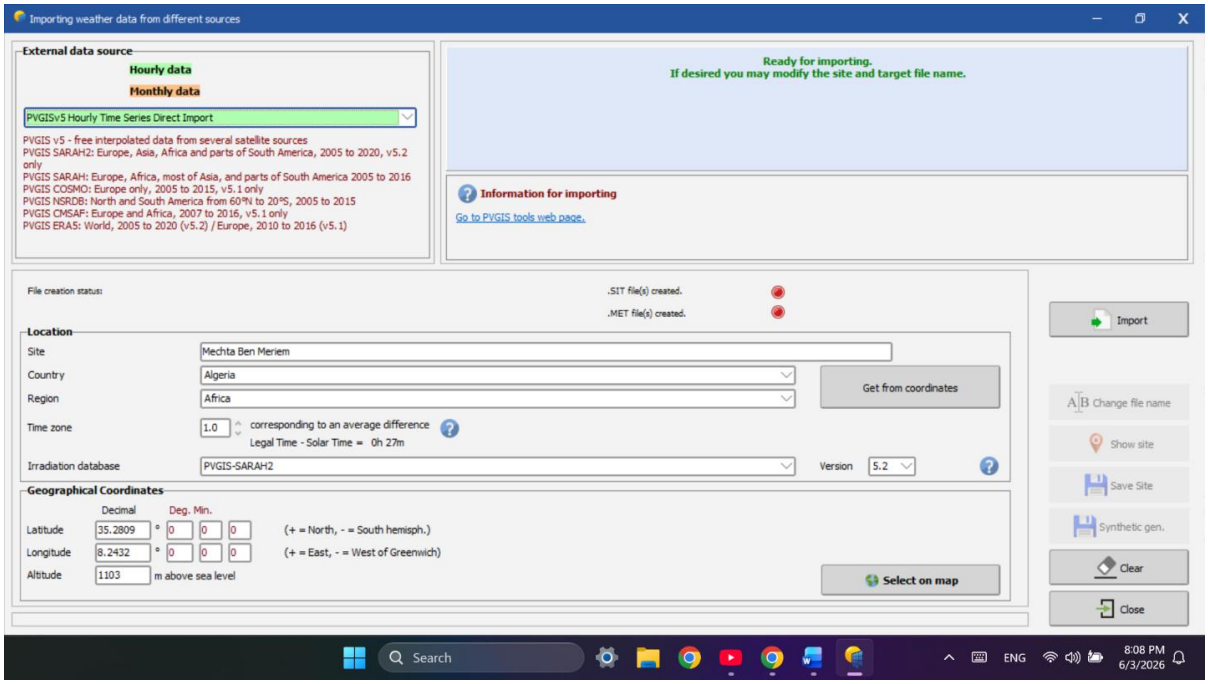


Figure III.4: Weather data import window – selection of the PVGIS-SARAH2 database

III.1.3 Orientation and tilt

In this step we must determine the PV array orientation and tilt to maximize solar energy acquisition. These parameters are displayed in Figure III.5 below.

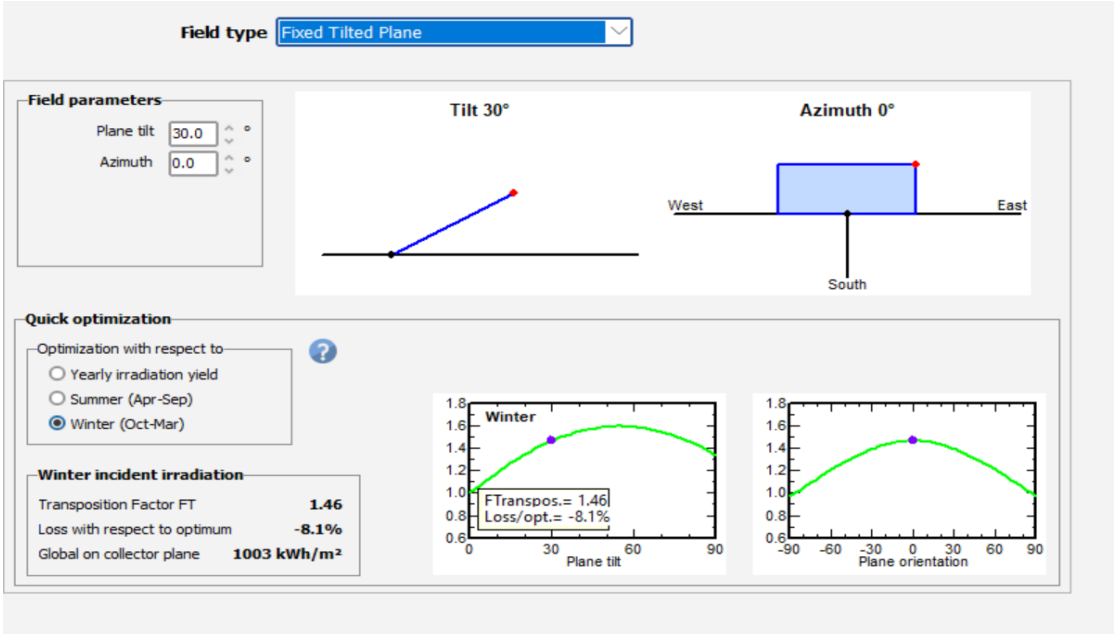


Figure III.5 PV array orientation and tilt optimization window.

III.1.4 Load needs

Creating a profile in the electrical load needs of the system (Figure III.6) is one of the major steps of the simulation. But since our system uses energy in a very intermittent regime and PVsyst does not allow for that kind of precise load distribution. The decision was made to use an average hourly consumption of 7.43Wh which results in a 178.34Wh/day or $1/3$ of the irrigation cycle energy needs per day.

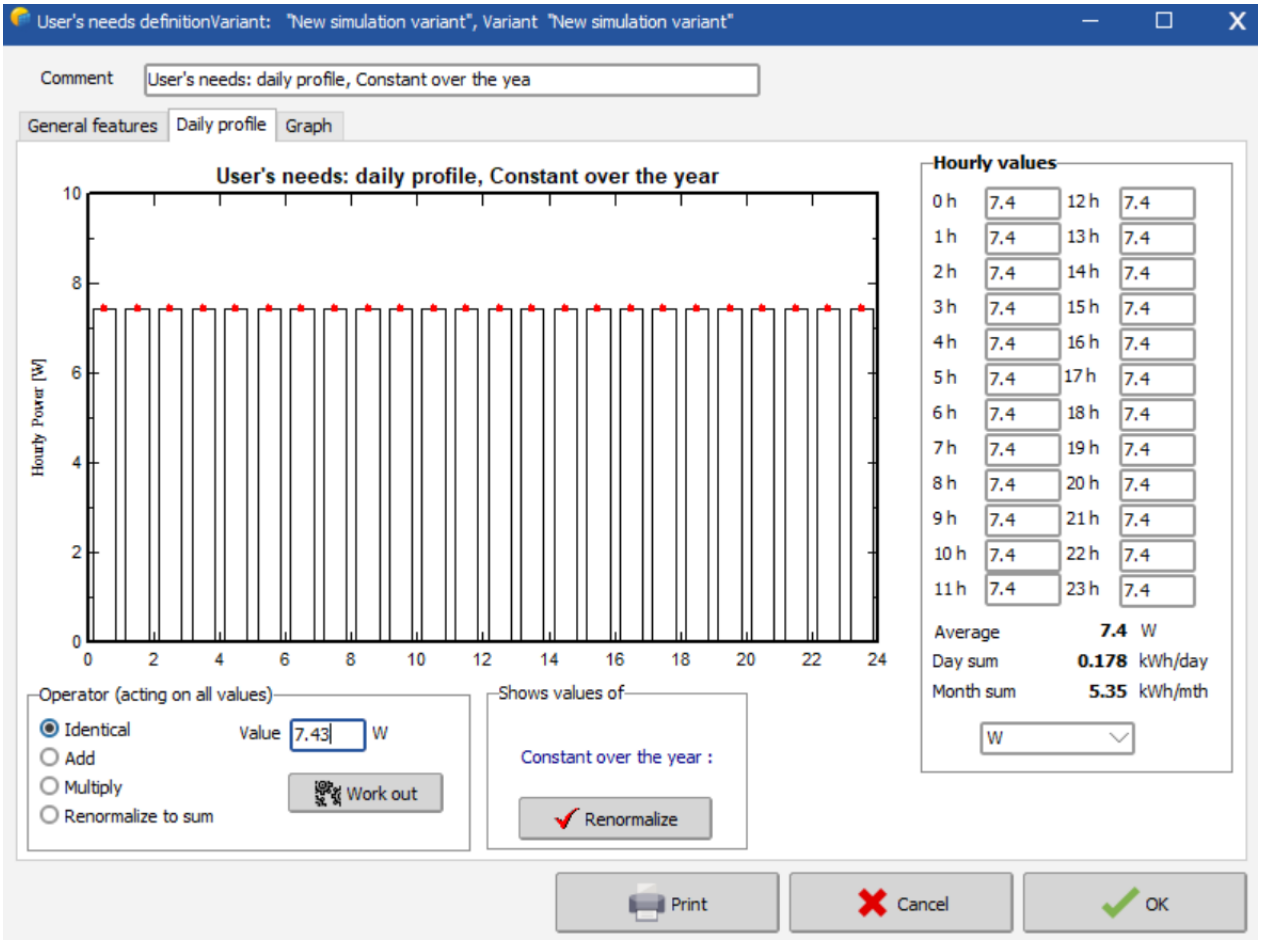


Figure III.6: Definition of the system's hourly load profile (average of 7.43 Wh).

III.1.5 Energy conversion and storage system

The energy conversion and storage system is split into two major steps which are choosing the storage system and the PV array.

III.1.5.1 Storage

Our chosen battery is not available in the database of the software, so we defined ours from the datasheet information as shown in Figure III.7 below.

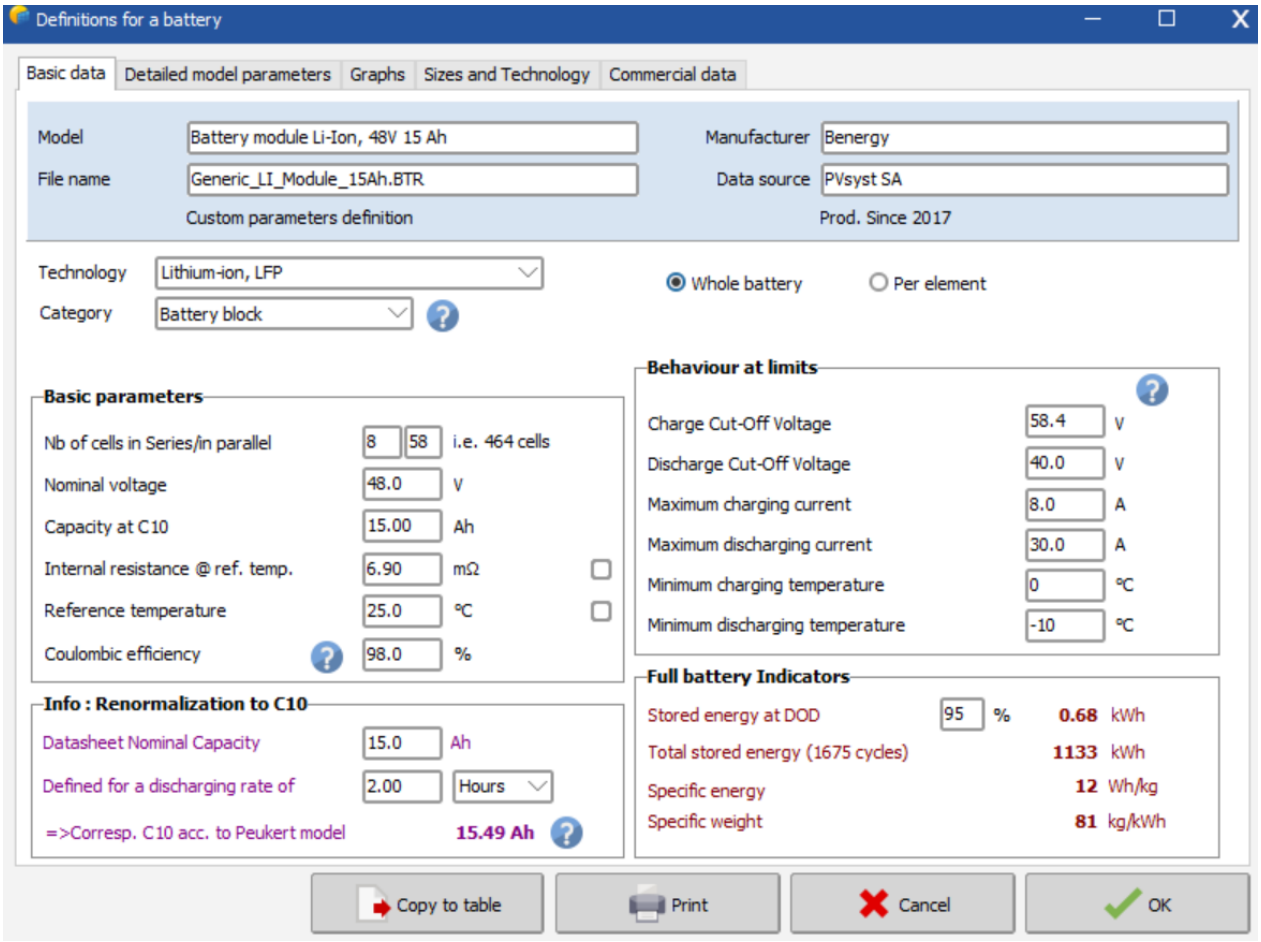


Figure III.7: Battery parameters entered from the manufacturer's datasheet.

Then we configure the whole battery set which has a single battery as the Figure III.8 shows .

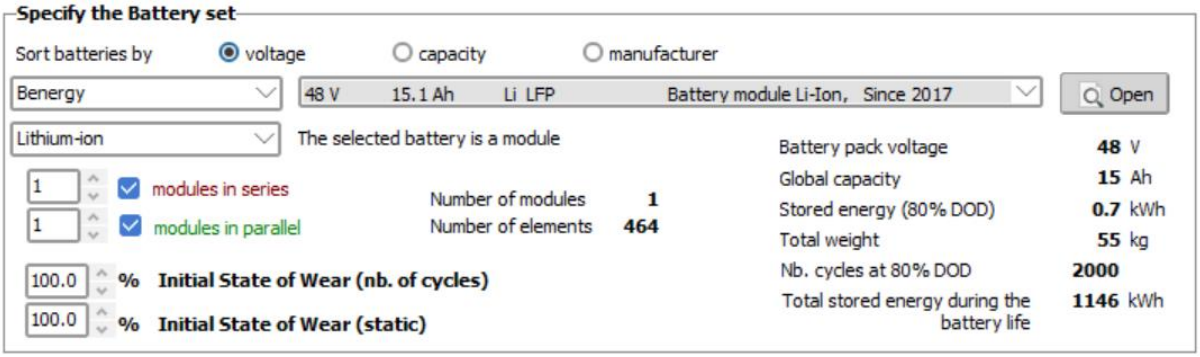


Figure III.8: Configuration of the battery pack.

III.1.5.2 The PV module

The chosen solar panel in the previous chapter is readily available in the software's database. So we select it (Figure III.9).

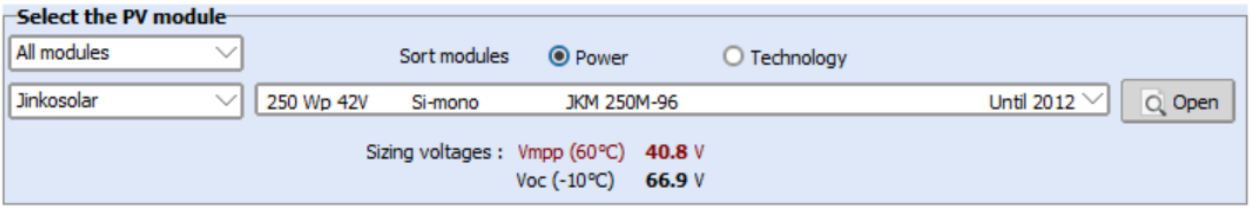


Figure III.9: Selection of the PV module in the PVsyst database.

III.1.5.3 MPPT charge regulator

We have selected the generic charge regulator built in the software (Figure III.10) and added the specification of the chosen regulator in the previous chapter .

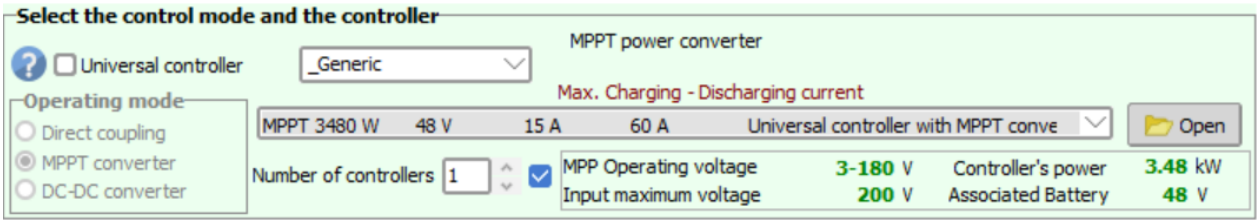


Figure III.10: Selection of the MPPT charge controller.

III.1.5.4 The PV array

The PV array is a single standalone module (Figure III.11).

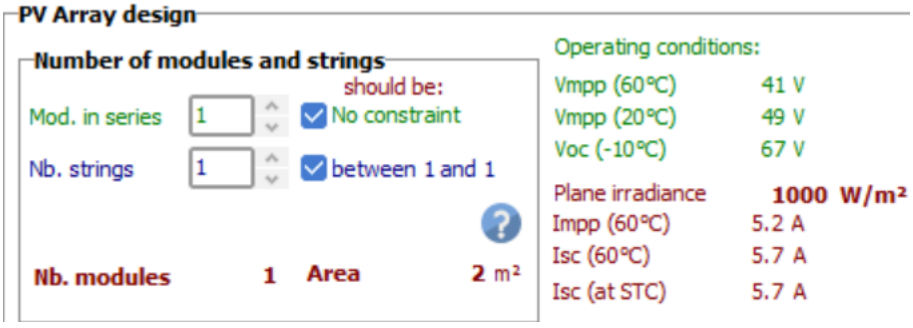


Figure III.11: Configuration of the PV array (modules per string and number of strings).

III.1.6 Simulation results

After running the simulation we got the following results. Which consists of the normalized energy production balance graph presented in Figure III.12 below.

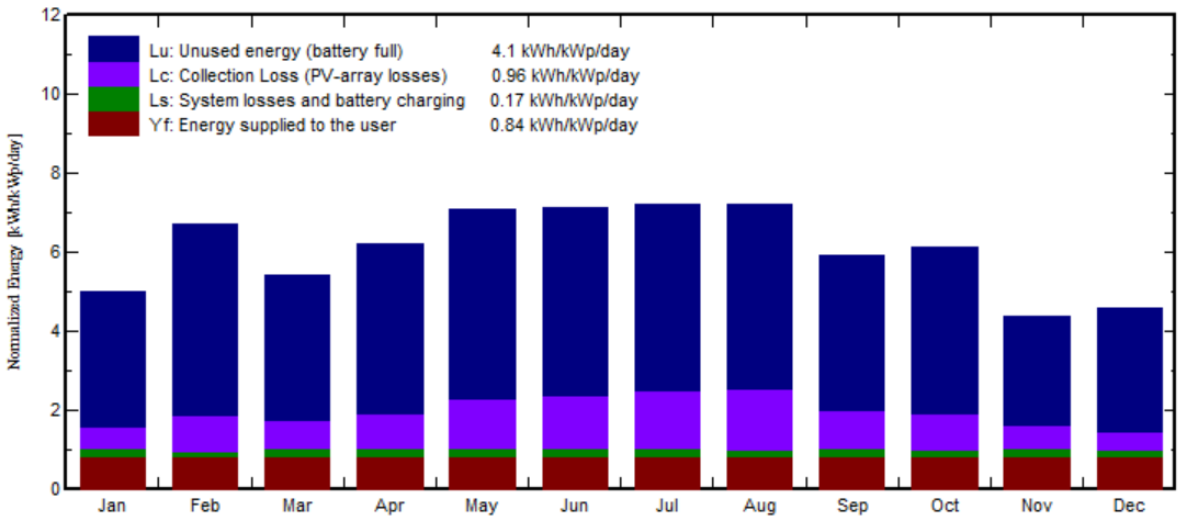


Figure III.12: Simulation results – normalized energy production balance.

III.1.6.2 Interpretation

This graph shows an average unused energy of 4.1 kwh/day, which is to be expected as the energy needs of the system are too low 0.178kwh/day. Nevertheless this kind of excess energy is to be expected due to the oversizing of the battery pack and the corresponding PV array. This oversizing is a consequence of the system's short term power requirements and limitation of the batteries maximum discharge current, and it have been explained thoroughly in the previous chapter.

III.2 PLC program using LOGO!Soft

Developed by the leaders in automation, Siemens. The LOGO! Soft is a user friendly software package used for programming, simulating, and configuring Siemens LOGO! programmable logic controllers (PLCs), Figure III.13 shows the software's interface. The LOGO! PLC is chosen because it has a built in screen, removing the need for an external HMI. It provides an intuitive graphical interface that allows users to create automation programs using function blocks and ladder diagrams without requiring advanced programming skills. Widely used in industrial, commercial, and educational applications, LOGO! Soft helps design and test control systems efficiently before deployment, reducing development time and improving system reliability.

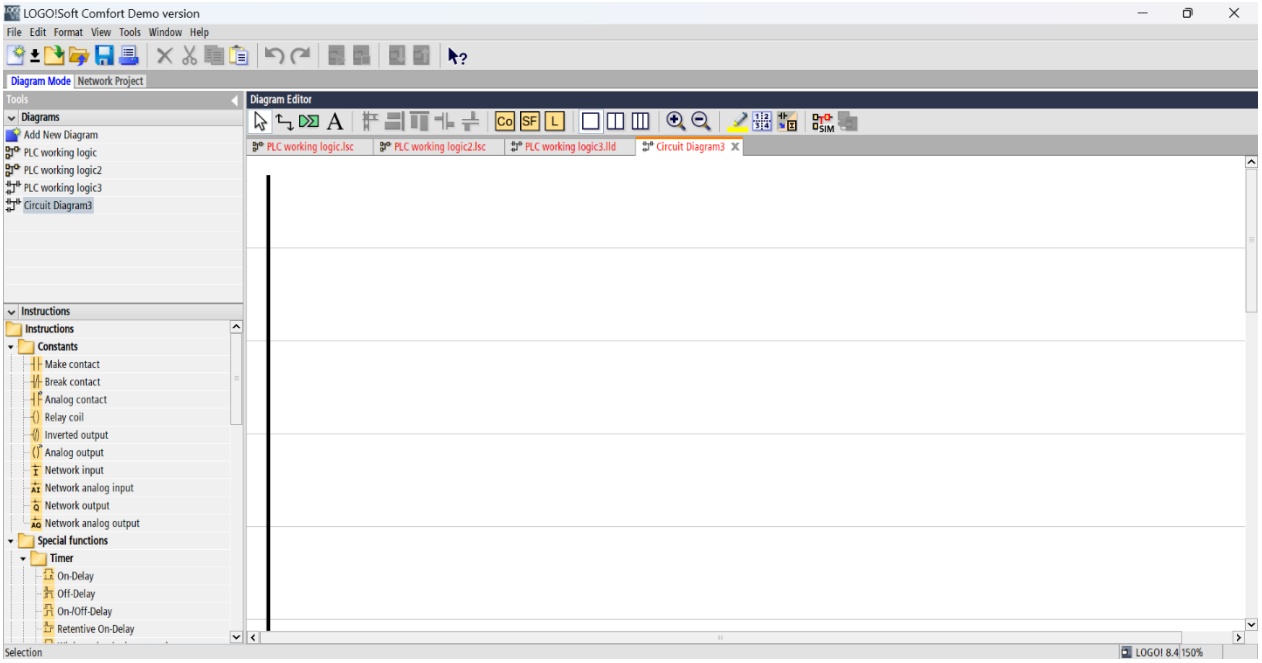


Figure III.13: LOGO!Soft Comfort programming interface.

Logo! Soft provides the user with two choices for writing the program, either by using the function block diagram FBD language editor or by using the Ladder language editor. Also the software can convert programs from one language to the other.

The used FBD blocks and their functions are presented in the Table III.1 below, And for the connections between the different blocks, it have been done based on the system's operational logic.

Table III.1: Function blocks used in the PLC program and their roles.

Function block	Parameter	Role
I1	Input	Start button
I2	Input	Stop button
Q1	Output	Forward motors direction
Q2	Output	Reverse motors direction
B001	RS latch	Sets and resets the M1 flag
B002	On-delay (24s)	Forward rotation duration
B003	On-delay (3h)	Pause duration
B004	Off-delay (540s)	Reverse rotation duration
B006	Up/Down counter (23 up)	Counts number of pauses per cycle.
M1	Flag	System on internal flag
M2	Flag	Forward direction internal flag
M3	Flag	Pause internal flag
M4	Flag	Reverse direction internal flag
B007 → B0013	AND	Logic operators

In our case we used the function block diagram FBD to simulate the logic of our system inside the PLC, Then we converted the program to Ladder for better visualization as shown in Figure III.14 below.

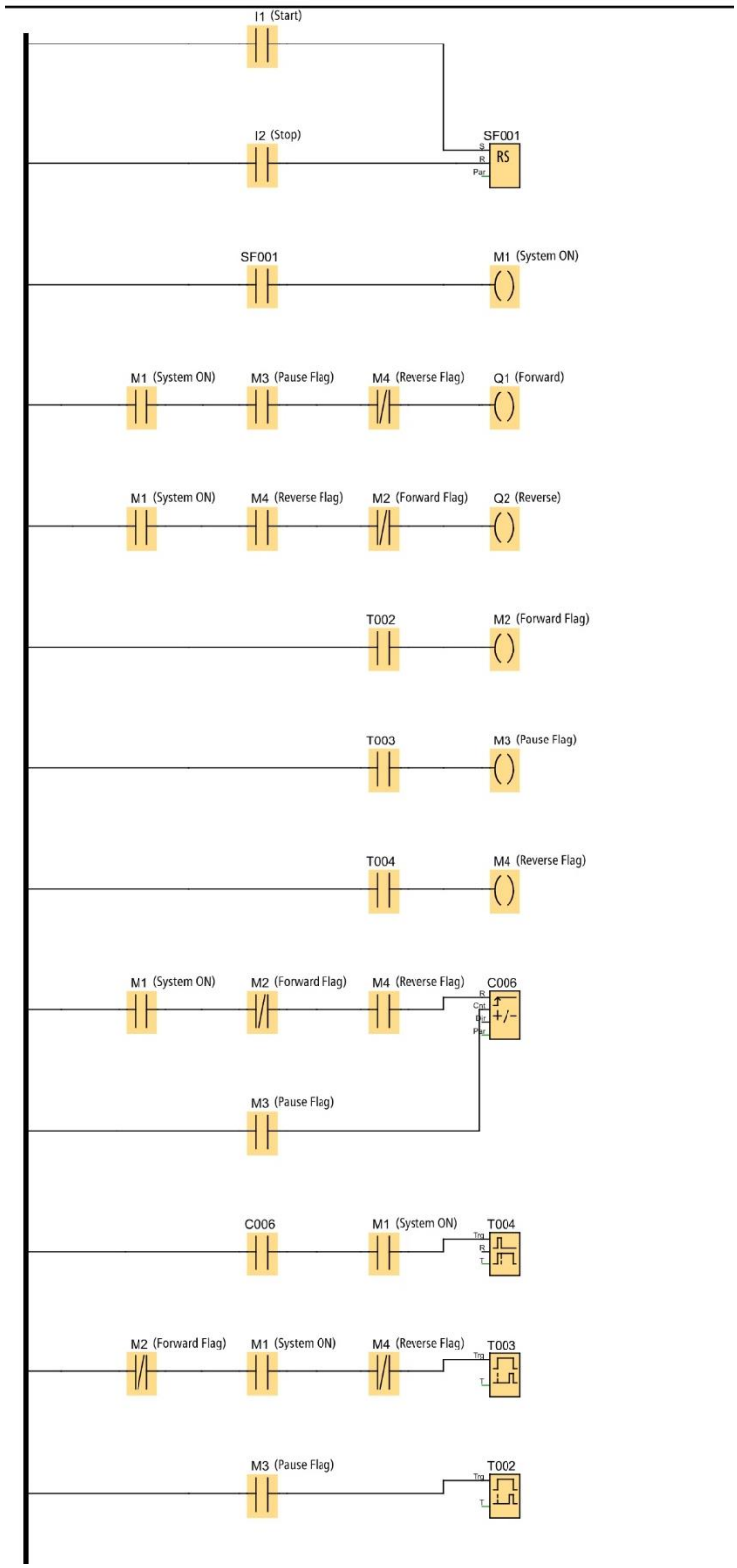


Figure III.14: Ladder diagram of the PLC control program.

III.3 System simulation using MATLAB/Simulink

MATLAB/Simulink is a computing, modeling, and simulation environment widely used in the study of electrical, electronic, and energy systems. It enables complex systems to be represented as block diagrams, facilitating the analysis of their dynamic behavior without requiring direct experimental implementation.

In the field of photovoltaics, Simulink allows for the modeling of various components of a solar installation, such as the photovoltaic array, static converters, batteries, inverters, and electrical loads. It also makes it possible to monitor key electrical parameters, notably voltage, current, power, and battery state of charge.

III.3.1 System overall model

Since we have presented the photovoltaic energy conversion and storage chain using PVsyst, And the system's logic was furthermore elaborated using LogoSoft!. It leaves only the power chain to be simulated using MATLAB/SIMULINK, which includes the path of the current flow going from the battery all the way to the DC-motor. The system's Model is presented in Figure III.15 below.

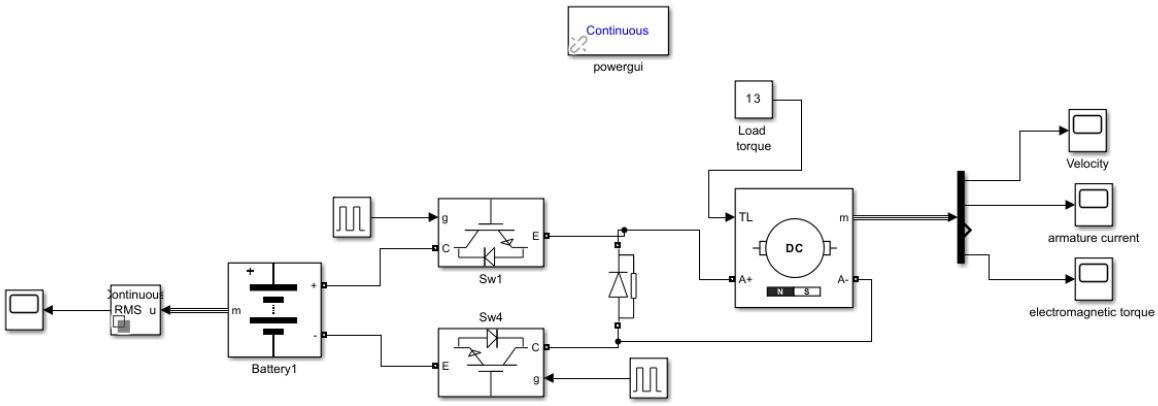


Figure III.15: Overall Simulink model of the system's power chain.

III.3.2 Battery block

The battery block (Figure III.16) implemented have the same characteristics as the battery pack established in chapter II.

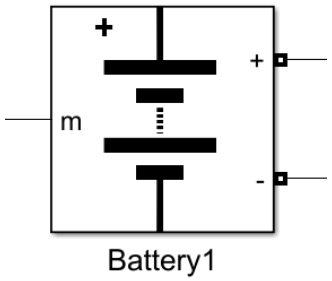


Figure III.16: Battery block used in the Simulink model.

III.3.3 Permanent magnet DC motor

We used the DC motor prebuilt in the Simscape library (Figure III.17), the motor's parameters were taken from the motor's datasheet presented in chapter II.

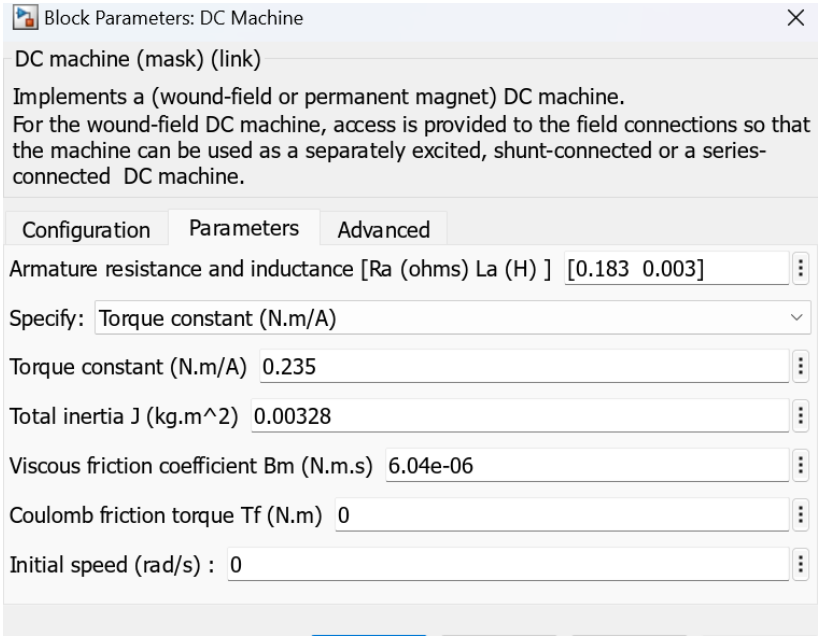


Figure III.17: Parameters of the permanent magnet DC motor block.

III.3.4 Motor drive controller

For the purposes of this simulation we have used two IGBT switches SW1 and SW4 to represent half the bridge or the first quadrant (forward motion). With an open loop control using a pulse generator, its duty cycle is 46.5% which corresponds to a motor speed output of 500rpm under a constant load of 13.5Nm.

The driver also includes an ideal freewheeling diode to compensate for the switches open state.

The driver's blocks are presented in Figure III.18 below.

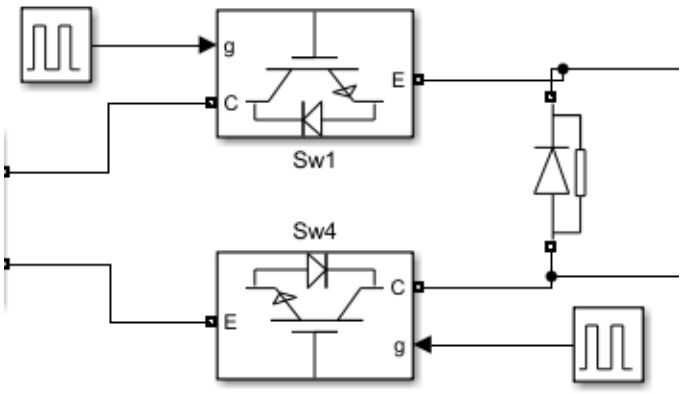


Figure III.18: Motor drive controller circuit (IGBT switches and freewheeling diode).

III.3.5 Simulation results

After running the simulation, with the working conditions that have been established in the previous chapter we have achieved the following results, represented in the graphs below as a function of time.

Figure III.19 below represents the motor's speed response under the established conditions during the simulation time of 0.5s.

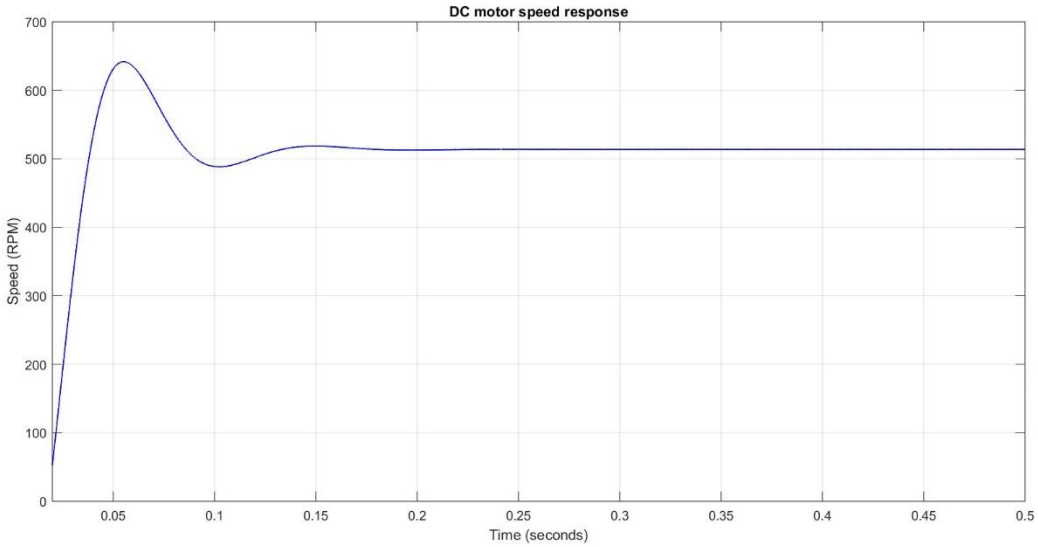


Figure III.19: Simulated DC motor speed response

Figure III.20 shows the motor's torque response in the startup phase and the established regime phase

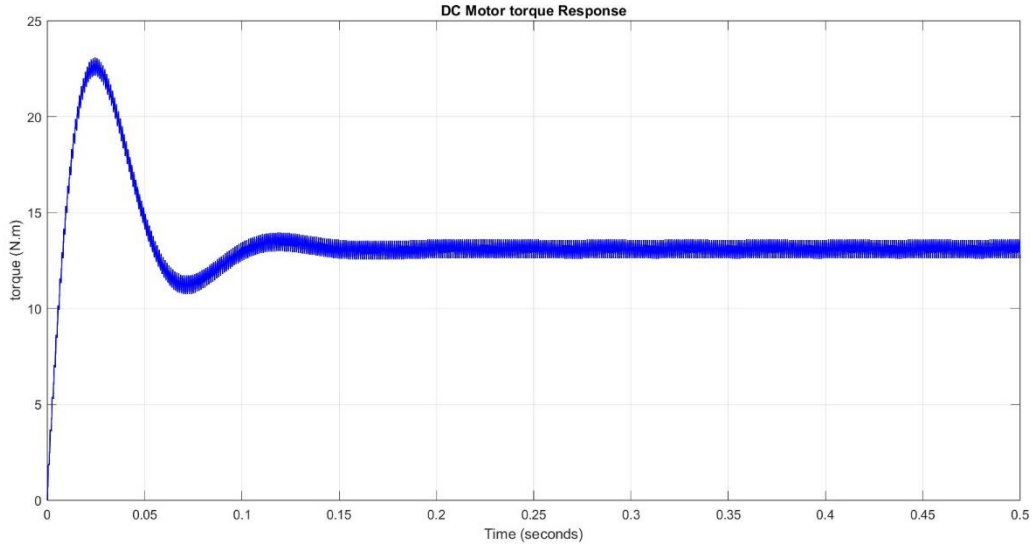


Figure III.20: Simulated DC motor torque response.

Figure III.21 represents the motor's armature current during operation from startup to the permanent regime.

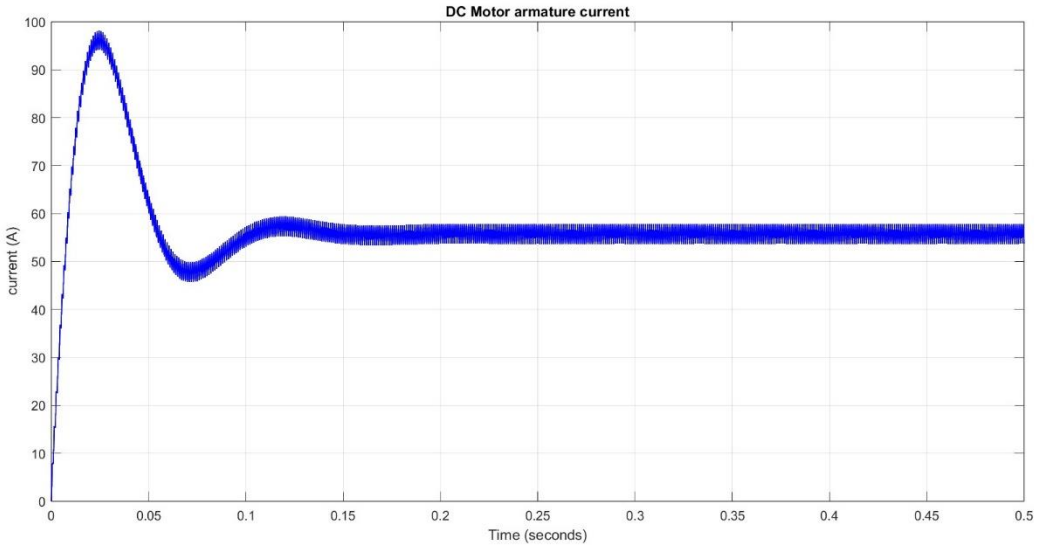


Figure III.21: Simulated DC motor armature current.

Figure III.22 is the measured current output of the battery during operation.

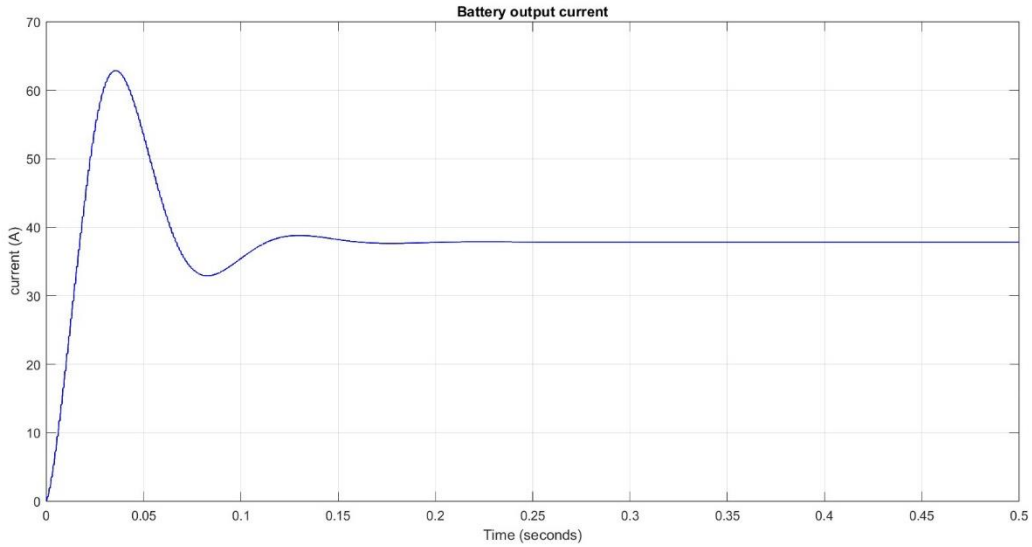


Figure III.22: Simulated battery output current.

III.3.6 Results interpretation

Given the constant torque of the load, the motor's stabilization took 0.2s. Also the startup torque of the motor reached twice the load torque which covers the stopped state torque requirement mentioned in chapter II.

The motor angular velocity stabilized at a constant speed of 510rpm which corresponds to the calculated theoretical speed of 500rpm (Figure III.19).

The motor's armature current peaked at a value of 93A during startup, and a constant RMS current of 56.8A after stabilization (Figure III.21).

The battery's output current peaked at a value of 62.9A during startup, and a constant RMS current of 37.8A after stabilization (Figure III.22).

III.4 Conclusion

Throughout this chapter, the different components of the irrigation system have been simulated using three complementary software tools. The PVsyst simulation confirmed that the photovoltaic generation and storage chain sized in the previous chapter is able to cover the system's energy needs, although it revealed a significant amount of unused energy resulting from the deliberate oversizing of the battery pack and PV array, made necessary by the system's short-term power requirements and the batteries' maximum discharge current. The LOGO!Soft simulation validated the PLC program implementing the system's control logic, based on the flow chart established in chapter two, and confirmed the correct sequencing of the forward rotation, pause and reverse rotation phases. Finally, the MATLAB/Simulink simulation of the power chain validated the dynamic behavior of the DC motor under load, showing a stabilization time of 0.2 s and a steady-state speed of 510 rpm, in good agreement with the theoretical value of 500 rpm calculated previously, together with acceptable startup current and torque peaks. Overall, the results obtained from the three simulation environments are consistent with one another and with the theoretical sizing carried out in the previous chapter, confirming the feasibility of the proposed system ahead of its practical implementation.

Chapter IV : Prototype

IV. Introduction

This chapter presents the design, implementation, and testing of the prototype developed to demonstrate the feasibility of a solar powered mobile platform intended for irrigation. The prototype was conceived as a **proof of concept**, and as such its purpose is not to deliver a deployable agricultural product, but rather to validate that a small autonomous solar charged vehicle can operate reliably using the logic demonstrated in chapter III

The prototype consists of a 3D-printed chassis and wheel assembly, a solar panel and charge controller feeding a 3.7 V battery, an Arduino Nano microcontroller, two continuous rotation servo motors driving the wheels directly, an on/off switch controlling the power circuit, and a water pipe mounted on the chassis for the irrigation function of the system. The vehicle operates on a simple, preprogrammed cycle, moving forward for a fixed duration, stopping, moving backward for a fixed duration then stopping again. With no external control input and no onboard sensing.

IV.2 System Overview

The prototype is organized around a straightforward power and control architecture, explained below:

Power is generated by the solar panel and regulated by the solar charge controller, which manages charging of the 3.7 V battery. The battery, once switched on via the on/off switch, supplies power to both the Arduino Nano and the two continuous rotation servo motors. The Arduino Nano executes a preprogrammed control sequence with no sensor feedback or external command input, driving the two servo motors which are coupled directly to the wheels. The water pipe is mounted on the chassis as a passive element representing the intended irrigation application of the platform, it is not actuated or connected to any control logic in this prototype.

This architecture was deliberately kept minimal, consistent with the proof of concept nature of the project, it isolates and demonstrates the core sub systems (solar energy harvesting, energy storage, and basic locomotion).

IV.3 Mechanical Design

IV.3.1 Chassis Design

The chassis of the prototype was produced using 3D printing, which was selected for its low cost, rapid iteration capability, and suitability for producing custom geometries that accommodate the electronic and power components used in the prototype.

It was designed with two end towers that house the electronic components, with a U shaped middle section to carry the water pipe and cables inside it and the solar panel above.

Overall chassis dimensions are 200mm×200mm×100mm (Figure IV.1)

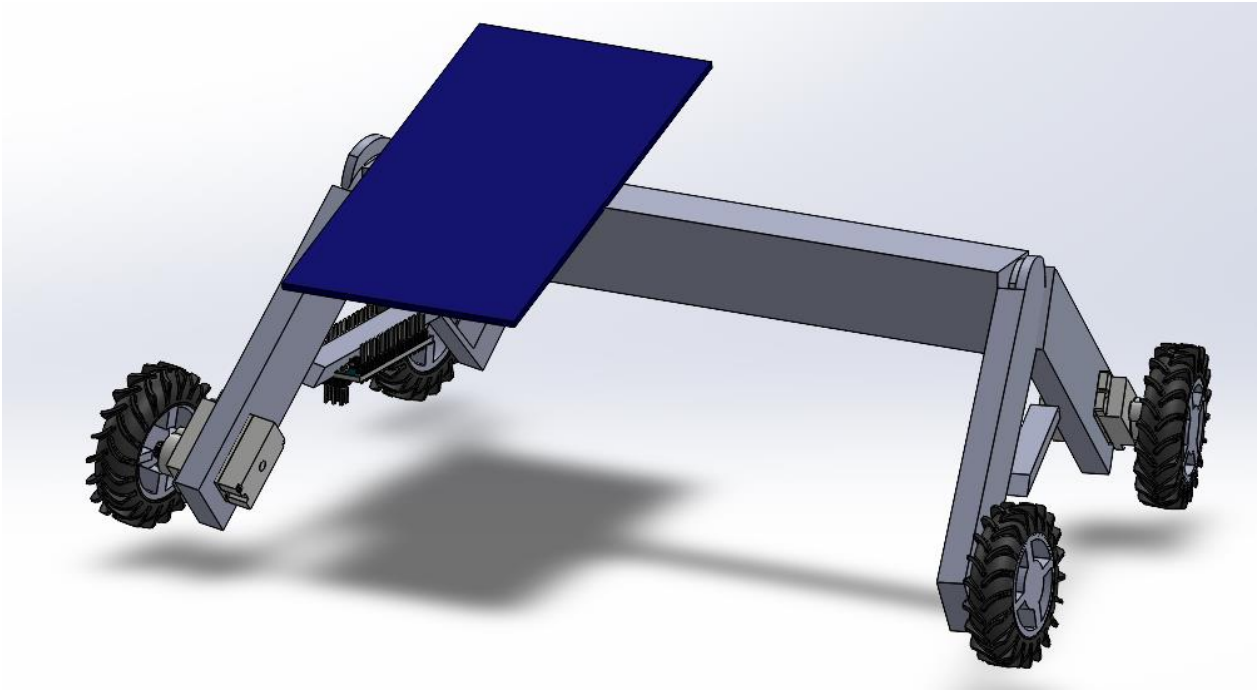


Figure IV.1: 3D model render of the prototype

IV.3.2 Wheels Design

The wheels were also 3D-printed, with a diameter of 45mm. The wheel hubs were designed to mount directly onto the output shaft of the continuous rotation servo motors, allowing direct drive without an intermediate gearbox or transmission (Figure IV.2).



Figure IV.2: 3D model render of the system wheels

The chassis also contains A water pipe, 6mm in diameter and 300 mm in length, representing the irrigation carrying function envisioned for a full scale version of this platform. The pipe also contains two secondary tubes mounted vertically to serve the sprinkler function.

IV.4 Power System Design

IV.4.1 Solar Panel Selection

The prototype uses a small solar panel (FigureIV.3) rated at 6V open circuit voltage and 210 mA under standard test conditions, selected primarily for its compact size relative to the chassis and its compatibility with the voltage requirements of the solar charge controller.[30]



Figure IV.3: 6V 210mA Solar panel

IV.4.2 Solar Charge Controller

A solar charge controller was placed between the solar panel and the battery to regulate the charging process and protect the battery from overcharging. The controller used is the CN3791 (Figure IV.4) which provides overvoltage and overcharge protection, it also has built in MPPT tracking which maximize the charging of the battery.[31]



Figure IV.4: the CN3791 solar charge regulator

This component was necessary because direct connection of the solar panel to the battery would risk overcharging the cell under strong sunlight, given that solar panel output voltage can exceed the safe charging voltage of a 3.7 V lithium-based cell.

IV.4.3 Battery Selection

The prototype is powered by a single 3.7 V lithium-ion battery cell with a rated capacity of 4800mAh (Figure IV.5). This chemistry and voltage were selected for its compatibility with the solar charge controller, favorable energy density for the given chassis volume and weight.



Figure IV.5: A 3.7 V lithium-ion battery cell

IV.5 Control System Design

IV.5.1 Microcontroller Selection

The Arduino Nano (Figure IV.6) was selected as the control unit for this prototype for the following reasons:

- **Compact form factor** : its small footprint of 45mm×18mm suited the limited space available on the 3D-printed chassis.
- **Sufficient I/O** : its digital pins were sufficient to generate the PWM control signals required by the two continuous-rotation servo motors, with headroom for future expansion.
- **Adequate processing capability** for the simple, timed, preprogrammed control loop required by this prototype, which does not involve sensor fusion, wireless communication, or complex computation.



Figure IV.6: Arduino Nano

IV.5.2 Continuous Rotation Servo Motors

Two continuous rotation servo motors were used to drive the wheels directly, one per tower, enabling differential style forward and reverse motion without an additional motor driver IC, since continuous rotation servos accept a standard PWM signal directly from the microcontroller's digital pins.

This choice was made over conventional DC motors with a separate motor driver due to the limited space in the chassis and the waterproof body of servo motors.

The servo motors used are rated at 4.8 V operating voltage and 2kg·cm stall torque (FigureIV.7). Direction and speed of rotation are controlled by varying the pulse width of the PWM signal sent from the Arduino Nano.[32]



Figure IV.7: continuous rotation Servo motor MG90s

IV.5.3 On/Off Switch

A physical on/off switch (Figure IV.8) was placed in series with the battery output to allow the entire circuit to be powered down without disconnecting the battery from the charge controller, so that solar charging can continue even while the vehicle itself is powered off. The switch used is a 3 pin SPDT 6A Toggle Switch.



Figure IV.8: 6A toggle switch

IV.6 Circuit Design and Wiring

The solar panel connects to the input terminals of the solar charge controller, which in turn connects to the 3.7 V battery. The battery's positive terminal is routed through the on/off switch before reaching the Arduino Nano's power input (VIN) and the power rails supplying the two servo motors. Figure IV.9 shows the complete schematic of the prototype's electrical system.

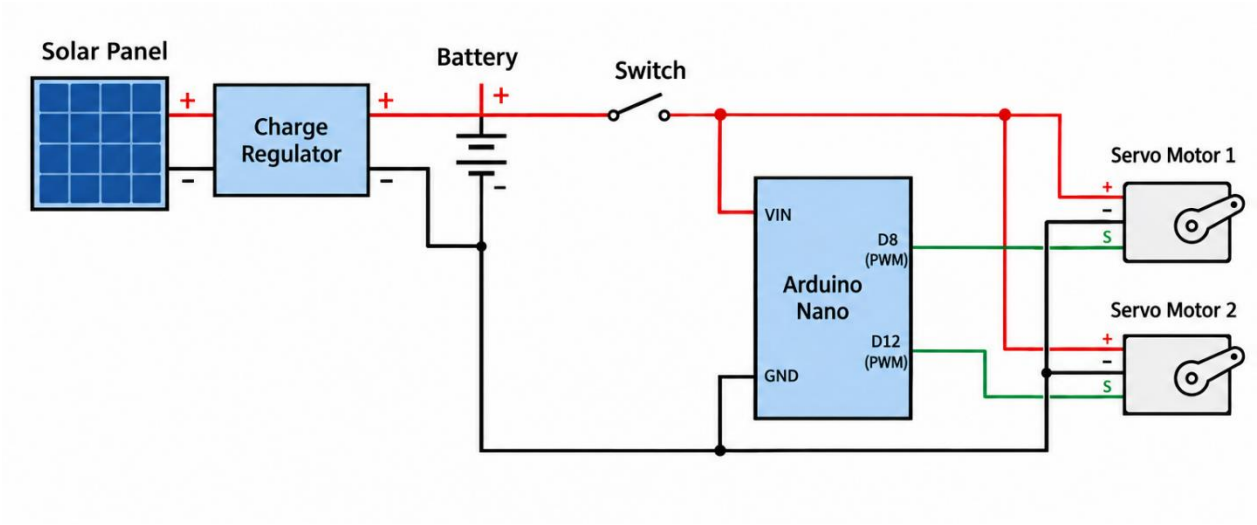


Figure IV.9: prototype wiring schematic

The following Table IV.1 shows the pins connected on the Arduino and the functions they serve.

Table IV.1 connected Pins on the Arduino and their function

PIN	Function
5V	Arduino power input
GND	Arduino ground pin
D8	PWM signal for the first motor
D12	PWM signal for the second motor

All grounds (Arduino Nano, servo motors, battery, charge controller) were tied to a common ground reference.

IV.7 Firmware Design

IV.7.1 Control Logic

The firmware running on the Arduino Nano implements a simple, preprogrammed time based control loop with no sensor feedback and no external command input. The vehicle cycles continuously through eight states:

1. Move forward for a fixed duration of 4 seconds.
2. Stop for a fixed duration of 5 seconds.
3. Move forward for a fixed duration of 4 seconds.
4. Stop for a fixed duration of 5 seconds.
5. Move backward for a fixed duration of 4 seconds.
6. Stop for a fixed duration of 5 seconds.

7. Move backward for a fixed duration of 4 seconds.
8. Stop for a fixed duration of 5 seconds.

After the final stop state, the sequence repeats indefinitely from step 1, for as long as the on/off switch keeps the circuit powered. Both servo motors are driven with the same PWM values during the forward and backward states, but with the pulse width of one motor mirrored relative to 1500 µs neutral, since the two motors are mounted facing opposite directions on the chassis and must therefore rotate in opposite senses to produce coordinated rather than opposing wheel rotation.

IV.8 Assembly and Final Prototype

The finished prototype (Figure IV.10) was assembled by first mounting the Arduino Nano, battery, solar charge controller, and on/off switch inside the 3D-printed chassis, followed by attachment of the two continuous rotation servo motors and wheels, then fixing the solar panel onto the chassis and finally the water pipe. Wiring between components followed the schematic presented previously

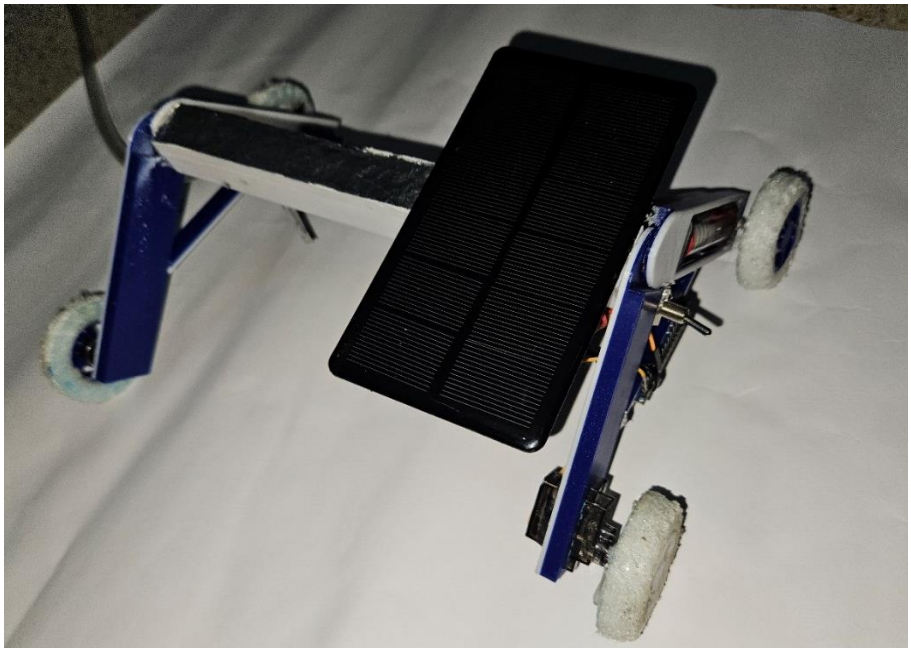


Figure IV.10: A picture of the finished prototype

IV.9 Limitations

The prototype, as a proof of concept, has a number of limitations that should be acknowledged:

- No sensing or feedback: the vehicle operates entirely open loop, with fixed timing for each movement phase. It cannot detect obstacles, correct its path, or adapt its behavior to the environment.
- Fixed-timing control: because movement durations are hard coded rather than derived from distance or position feedback, actual distance traveled per phase may vary with terrain, battery charge level, or servo wear.

IV.10 Conclusion

This chapter presented the design and implementation of a solar powered, automatic irrigation traction prototype intended as a proof of concept for a low cost irrigation support platform. The prototype successfully integrated solar energy harvesting, battery storage, a simple microcontroller based control system, and direct drive locomotion within a compact, 3D-printed chassis. And demonstrated repeatable, preprogrammed movement powered entirely by solar charged energy.

Based on the limitations identified in Section IV.9, some recommendation can be proposed to improve this prototype for future work, such as adding sensors and feedback to turn the system into closed loop operation for better control in different types of terrain.

General conclusion

General Conclusion and perspectives

This thesis set out to determine whether the movement of a lateral move irrigation machine could be reliably powered by photovoltaic panels and a lithium ion battery instead of a diesel generator or trailing cable, and to develop a methodology general enough to size such a system for a real site. The four chapters of this work build toward an affirmative answer to that question.

The literature review established that irrigation is central to global food security and to Algeria's water and energy policy in particular, and that while photovoltaic-powered pivot drives had already been studied, no prior work had addressed a lithium-buffered lateral move machine — the specific gap this thesis fills. Building on this, a modular design methodology was developed that decomposes the machine into identical repeating nodes, allowing the mechanical load, motor torque, and power requirements to be derived once and reused regardless of the overall machine length. Applied to a real 270 m × 150 m potato field in Mechta Ben Meriem, this methodology produced a fully specified drivetrain, a 48V 15Ah LiFePO4 battery, and a photovoltaic array sized to the site's worst-case irradiance conditions.

This sizing was then cross-validated using three independent simulation tools. The PVsyst simulation confirmed that the photovoltaic and storage chain comfortably covers the system's energy needs, at the cost of a significant, but deliberate and explainable, oversizing driven by the battery's maximum discharge current rather than by its energy capacity. The LOGO!Soft Comfort simulation confirmed the correct sequencing of the forward motion, pause and reverse motion logic that governs the machine's automatic control. The MATLAB/Simulink simulation of the motor and battery under load showed a stabilization time of 0.2 s and a steady-state speed of 510 rpm, in close agreement with the theoretical value of 500 rpm, together with acceptable startup current and torque peaks. The consistency of these three independent results substantially strengthens confidence in the design. Finally, a small-scale proof-of-concept prototype, built around an Arduino Nano, continuous-rotation servo motors, and a small solar-charged lithium cell, physically demonstrated repeatable, preprogrammed movement powered entirely by solar-charged energy, translating the simulated behavior into a tangible, working system.

Taken together, these results confirm that a photovoltaic and lithium-battery powered drive is a technically feasible and consistently validated alternative to diesel or cable power for lateral move irrigation machines, addressing a real and, in the Algerian Saharan context, increasingly urgent

need. The work also has clear limitations that point directly to future development: the prototype operates entirely open-loop, with fixed movement timings and no sensing or feedback, so its actual displacement can drift with terrain, battery charge level, or servo wear. The most natural extension of this work is therefore to close that loop adding position or distance feedback so that the system can correct its own movement and, at full scale, to extend the modular sizing methodology developed here to machines of different lengths, field geometries, and crop water requirements.

Bibliographic References

Bibliographic references

[1] FAO, IFAD, UNICEF, WFP, and WHO, *The State of Food Security and Nutrition in the World 2025*. Rome, Italy: FAO, 2025. [Online]. Available: https://www.fao.org/statistics/highlights-archive/highlights-detail/5/en

[2] D. L. Bjorneberg, "Irrigation | Methods," in *Reference Module in Earth Systems and Environmental Sciences*. Amsterdam, The Netherlands: Elsevier, 2013, doi: 10.1016/B978-0-12-409548-9.05195-2.

[3] FAO, *The State of Food and Agriculture 2020: Overcoming Water Challenges in Agriculture*. Rome, Italy: FAO, 2020. [Online]. Available: https://openknowledge.fao.org/bitstreams/4680d28b-6b4c-4b82-a2de-0d356d3306be/download

[4] FAO, "Water efficiency, productivity and sustainability in the NENA regions (WEPS-NENA): Algeria—Background and sites." [Online]. Available: https://www.fao.org/in-action/water-efficiency-nena/countries/algeria/background-and-sites/en

[5] "Agriculture in Algeria," Djazagro. [Online]. Available: https://www.djazagro.com/en/news-trends/studies-trends/agriculture-in-algeria

[6] T. Hartani, S. Idda, and F. Z. Bouras, "From water stress to food security: The remarkable greening of neo-irrigated Saharan areas in Algeria," in *Irrigation and Sustainability*, S. N. Kulshreshtha, Ed. London, U.K.: IntechOpen, 2026, doi: 10.5772/intechopen.1016660.

[7] "A turning point for Algerian solar," *pv magazine*, Nov. 5, 2024. [Online]. Available: https://www.pv-magazine.com/2024/11/05/a-turning-point-for-algerian-solar-2/

[8] "Center pivots: Innovation that grew crops and acres in Nebraska," *CropWatch*, Univ. Nebraska–Lincoln, 2024. [Online]. Available: https://cropwatch.unl.edu/2024/center-pivots-innovation-grew-crops-and-acres-nebraska/

[9] R. F. Reinke and R. J. Coash, “Guidance system for lateral move irrigation machines,” U.S. Patent 4 463 906, Aug. 7, 1984. [Online]. Available: https://patents.google.com/patent/US4463906

[10] Van den Bussche, “Zimmatic 9500PL lateral move,” Product sheet. [Online]. Available: https://vandenbussche.com/product-sheet/zimmatic-9500pl-lateral-move

[11] Freie Universität Berlin, "Linear move irrigation system," IWRM teaching material (citing T. Scherer, 2010). [Online]. Available: https://www.geo.fu-berlin.de/en/v/iwrm/Implementation/technical_measures/Irrigation-systems/sprinkler/linear_move/index.html

[12] J. I. Herraiz, R. H. Almeida, M. Castillo-Cagigal, and L. Narvarte, "Experimental performance evaluation of a PV-powered center-pivot irrigation system for a three-year operation period," *Energies*, vol. 16, no. 9, Art. no. 3654, Apr. 2023, doi: 10.3390/en16093654.

[13] D. Berwanger, S. W. Haupenthal, J. A. C. Siqueira, and M. A. Vilas Boas, "Energia solar fotovoltaica autônoma na irrigação por pivô central [Photovoltaic solar energy in central pivot irrigation]," *Res., Soc. Dev.*, vol. 13, no. 7, Art. no. e7813746354, 2024, doi: 10.33448/rsd-v13i7.46354.

[14] W. Yantren and A. Bouzouidja, "Étude des performances d'un générateur photovoltaïque alimentant un système d'irrigation à pivot central," M.S. thesis (Mécanique, Énergétique), Faculté de Technologie, Univ. Saad Dahlab Blida 1, Blida, Algeria, 2023. [Online]. Available: https://di.univ-blida.dz/jspui/bitstream/123456789/25947/1/

[15] A. Luque and S. Hegedus, Eds., *Handbook of Photovoltaic Science and Engineering*, 2nd ed. Chichester, U.K.: Wiley, 2011.

[16] M. Mostefaoui, A. Ziane, A. Bouraiou, and S. Khelifi, "Effect of sand dust accumulation on photovoltaic performance in the Saharan environment: Southern Algeria (Adrar)," *Environ. Sci. Pollut. Res.*, vol. 26, pp. 259–268, 2019, doi: 10.1007/s11356-018-3496-7.

[17] T. Esram and P. L. Chapman, "Comparison of photovoltaic array maximum power point tracking techniques," *IEEE Trans. Energy Convers.*, vol. 22, no. 2, pp. 439–449, Jun. 2007, doi: 10.1109/TEC.2006.874230.

[18] Battery University, "BU-216: Summary table of lithium-based batteries," Cadex Electronics, last updated Oct. 25, 2021. [Online]. Available: https://batteryuniversity.com/article/bu-216-summary-table-of-lithium-based-batteries

[19] M. A. Hannan, M. S. H. Lipu, A. Hussain, and A. Mohamed, "A review of lithium-ion battery state of charge estimation and management system in electric vehicle applications:

Challenges and recommendations," *Renew. Sustain. Energy Rev.*, vol. 78, pp. 834–854, Oct. 2017.

[20] N. P. Widodo, S. Kramadibrata, A. Rohman, Y. Wicaksana, and F. Hermawan, “Rolling resistance study of gravelly sand material on laboratory scale,” Available: https://www.researchgate.net/publication/280239942_Rolling_Resistance_study_of_gravelly_sand_material_on_laboratory_scale

[21] World Bank Group and Solargis, “Global Solar Atlas.” Accessed: Sep. 20, 2026 [Online]. Available: https://globalsolaratlas.info/detail?s=35.323607,8.228684&m=site&c=35.284878,8.243637,11

[22] Maiak-M, “Calculator for seamless steel pipes – Circular.” Accessed: Sep. 20, 2026. [Online]. Available: https://www.maiak-m.bg/en/calculator/i2/Seamless-steel-pipes-circular.html

[23] TyreDekho, “Tyre weight across different kinds of vehicles,” CarDekho. Accessed: Sep. 26, 2026. [Online]. Available: https://tyres.cardekho.com/news/how-much-does-a-tyre-weigh-for-different-kinds-of-vehicles-fully-explained

[24] Leeson Electric, “109102.00 DataPack,” Specification sheet. Accessed: Sep. 20, 2026. [Online]. Available: https://cdn.lsicloud.net/kendall/Resources/AD/LEESON_109102_00_Specification_Sheet.pdf

[25] Guomaolide, “Understanding planetary gearbox efficiency: What you need to know in 2026,” Mar. 6, 2026. Accessed: Sep. 20, 2026. [Online]. Available: https://www.guomaolide.com/2026/03/06/understanding-planetary-gearbox-efficiency-what-you-need-to-know-in-2026/

[26] Angst+Pfister Sensors and Power, “MDC1xxx series,” Datasheet 1691-21588-0012-E-0219. Accessed: Sep. 20, 2026. [Online]. Available: https://sensorsandpower.angst-pfister.com/fileadmin/products/datasheets/230/Mdc1xxx_1691-21588-0012-E-0219.pdf

[27] Benergy Tech Co., Ltd., “E scooter 48V 15Ah lithium ion battery 2500 cycles 1500W IP63.” Accessed: Sep. 26, 2026. [Online]. Available:

https://www.lifepo4batterycells.com/sale-13885353-e-scooter-48v-15ah-lithium-ion-battery-2500-cycles-1500w-ip63.html

[28] LiTime, “LiTime 60A MPPT solar charge controller – High efficiency.” Accessed: Sep. 20, 2026. [Online]. Available: https://www.litime.com/products/60a-mppt-with-bluetooth

[29] JinKo Solar, “JKM155–240W mono: Technical specifications,” Datasheet. Accessed: Sep. 20, 2026. [Online]. Available: https://www.solarblitz.ch/datenblaetter/JinKo_JKM155-240W_mono.pdf

[30] AliExpress, “Mini 6V solar panel 1.25W with charger CN3065.” Accessed: Sep. 26, 2026. [Online]. Available: https://ar.aliexpress.com/item/1005008054346203.html?gatewayAdapt=glo2ara

[31] Consonance Electronic, “CN3791 datasheet,” alldatasheet.com. Accessed: Sep. 21, 2026. [Online]. Available: http://www.alldatasheet.com/datasheet-pdf/view/1132685/CONSONANCE/CN3791.html

[32] alhammadi-ye.com, "MG90S metal gear micro servo motor (180°/360°)," Datasheet. Accessed: Sep. 26, 2026. [Online]. Available: https://alhammadi-ye.com/public/uploads/all/w4y69MJcUpc26lvugrUjU1z1trfZCiVDSQSoW2an.pdf